4

Polymer Blends and Block Copolymers

A large part of applications oriented research is devoted to the study of polymer blends, since mixing opens a route for a combination of different properties. Take, for example, the mechanical performance of polymeric products. In many cases one is searching for materials that combine high stiffness with resistance to fracture. For the majority of common polymers these two requirements cannot be realized simultaneously, because an increase in stiffness, i.e., the elastic moduli, is usually associated with samples becoming more brittle and decreasing in strength. Using mixtures offers a chance to achieve good results for both properties. High-impact polystyrene, a mixture of polystyrene and polybutadiene, represents a prominent example. Whereas polystyrene is stiff but brittle, a blending with rubbers furnishes a tough material that still retains a satisfactory stiffness. Here mixing results in a two-phase structure with rubber particles of spherical shape being incorporated in the matrix of polystyrene. Materials are tough, if fracture energies are high due to yield processes preceding the ultimate failure, and these become initiated at the surfaces of the rubber spheres where stresses are intensified. On the other hand, inclusion of rubber particles in the polystyrene matrix results in only a moderate reduction in stiffness. Hence, the blending yields a material with properties that in many situations are superior to pure polystyrene. There are other cases, where an improvement of the mechanical properties is achieved by a homogeneous mixture of two polymers, rather than a two-phase structure. A well-known example is again given by polystyrene when blended with poly(phenyleneoxide). In this case, a homogeneous phase is formed and as it turns out in mechanical tests, it also exhibits a satisfactory toughness together with a high elastic modulus.

It is generally very difficult or even impossible to predict the mechanical properties of a mixture; however, this is only the second step. The first problem is an understanding of the mixing properties, i.e., a knowledge of under which conditions two polymeric compounds will form either a homogeneous phase or a two-phase structure. In the latter case, it is important to see how structures develop and how this can be controlled. This section deals

with these topics. We shall first discuss the thermodynamics of mixing of two polymers and derive equations that can be used for the setting-up of phase diagrams. Subsequently we shall be concerned with the kinetics of unmixing and here, in particular, with a special mode known as spinodal decomposition.

4.1 The Flory–Huggins Treatment of Polymer Mixtures

Flory and Huggins devised a general scheme that enables one to deal with the mixing properties of a pair of polymers. It provides a basic understanding of the occurrence of different types of phase diagrams, in dependence on temperature and the molar masses.

The mixing properties of two components may generally be discussed by considering the change in the Gibbs free energy. Figure 4.1 addresses the situation and introduces the relevant thermodynamic variables. Let us assume that we have $\tilde{n}_\mathrm{A}$ moles of polymer A, contained in a volume $\mathcal{V}_\mathrm{A}$ and $\tilde{n}_\mathrm{B}$ moles of polymer B, contained in a volume $\mathcal{V}_\mathrm{B}$. Mixing may be initiated by removing the boundary between the two compartments, so that both components can expand to the full volume of size $\mathcal{V} = \mathcal{V}_\mathrm{A} + \mathcal{V}_\mathrm{B}$. In order to find out whether a mixing would indeed occur, the change in the Gibbs free energy has to be considered. This change, called the **Gibbs free energy of mixing** and denoted $\Delta\mathcal{G}_\mathrm{mix}$, is given by

$$\Delta\mathcal{G}_\mathrm{mix} = \mathcal{G}_\mathrm{AB} - (\mathcal{G}_\mathrm{A} + \mathcal{G}_\mathrm{B}) \,, \tag{4.1}$$

where $\mathcal{G}_\mathrm{A}, \mathcal{G}_\mathrm{B}$ and $\mathcal{G}_\mathrm{AB}$ denote the Gibbs free energies of the compounds A and B in separate states and the mixed state, respectively. Employing the Gibbs, rather than the Helmholtz, free energy allows one to also include volume changes in the treatment, which may accompany a mixing at constant pressure. However, since the related term $p\Delta\mathcal{V}$ is always negligible, this is only a formal remark.

The **Flory–Huggins treatment** represents $\Delta\mathcal{G}_\mathrm{mix}$ as a sum of two contributions

$$\Delta\mathcal{G}_\mathrm{mix} = -T\Delta\mathcal{S}_\mathrm{t} + \Delta\mathcal{G}_\mathrm{loc} \,, \tag{4.2}$$

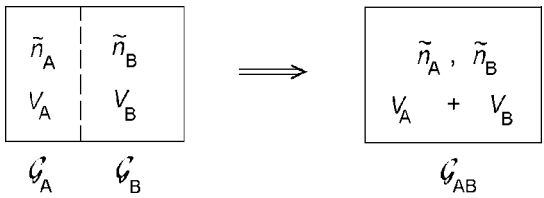

Fig. 4.1. Variables used in the description of the process of mixing of two polymers, denoted A and B

which describe the two main aspects of the mixing process. Firstly, mixing leads to an increase of the entropy associated with the motion of the centers of mass of all polymer molecules, and secondly, it may change the local interactions and motions of the monomers. We call the latter part $\Delta\mathcal{G}_{\mathrm{loc}}$ and the increase in the **translational entropy** $\Delta\mathcal{S}_{\mathrm{t}}$. $\Delta\mathcal{S}_{\mathrm{t}}$ and the related decrease $-T\Delta\mathcal{S}_{\mathrm{t}}$ in the Gibbs free energy always favor a mixing. $\Delta\mathcal{G}_{\mathrm{loc}}$, on the other hand, may act favorably or unfavorably, depending on the character of the monomer–monomer pair interactions. In most cases, and, as can be verified, for van der Waals interactions generally, attractive energies between equal monomers are stronger than those between unlike pairs. This behavior implies $\Delta\mathcal{G}_{\mathrm{loc}} > 0$ and therefore opposes a mixing. As a free energy, $\Delta\mathcal{G}_{\mathrm{loc}}$ also accounts for changes in the entropy due to local effects. For example, a shrinkage or an expansion of the total volume on mixing results in a change in the number of configurations available for local motions of the monomeric units, hence in a change of entropy to be included in $\Delta\mathcal{G}_{\mathrm{loc}}$.

The decomposition of $\Delta\mathcal{G}_{\mathrm{mix}}$ in these two contributions points to the two main aspects of the mixing process, but this alone would not be of much value. What is needed for actual use are explicit expressions for $\Delta\mathcal{S}_{\mathrm{t}}$ and $\Delta\mathcal{G}_{\mathrm{loc}}$, so that the sum of the two contributions can be calculated. The Flory–Huggins treatment is based on approximate equations for both parts. We formulate them first and then discuss their origins and the implications. The equations have the following forms:

1. The increase in the translational entropy is described by

$$\frac{\Delta\mathcal{S}_{\mathrm{t}}}{\tilde{R}} = \tilde{n}_{\mathrm{A}} \ln \frac{\mathcal{V}}{\mathcal{V}_{\mathrm{A}}} + \tilde{n}_{\mathrm{B}} \ln \frac{\mathcal{V}}{\mathcal{V}_{\mathrm{B}}} \,. \tag{4.3}$$

   Introducing the volume fractions ϕ_{A} and ϕ_{B} of the two components in the mixture, given by

$$\phi_{\mathrm{A}} = \frac{\mathcal{V}_{\mathrm{A}}}{\mathcal{V}} \quad \text{and} \quad \phi_{\mathrm{B}} = \frac{\mathcal{V}_{\mathrm{B}}}{\mathcal{V}} \,, \tag{4.4}$$

   $\Delta\mathcal{S}_{\mathrm{t}}$ can be written as

$$\frac{\Delta\mathcal{S}_{\mathrm{t}}}{\tilde{R}} = -\tilde{n}_{\mathrm{A}} \ln \phi_{\mathrm{A}} - \tilde{n}_{\mathrm{B}} \ln \phi_{\mathrm{B}} \,. \tag{4.5}$$

2. The change in the local interactions is expressed by the equation

$$\Delta\mathcal{G}_{\mathrm{loc}} = \tilde{R}T \frac{\mathcal{V}}{\tilde{v}_{\mathrm{c}}} \chi \phi_{\mathrm{A}} \phi_{\mathrm{B}} \,. \tag{4.6}$$

   It includes two parameters. The less important one is $\tilde{v}_{\mathrm{c}}$, denoting the (molar) volume of a reference unit common to both polymers. Principally it can be chosen arbitrarily, but usually it is identified with the volume occupied by one of the monomeric units. The decisive factor is the **Flory–Huggins parameter** χ. It is dimensionless and determines in empirical manner the change in the local free energy per reference unit.

What is the physical background of these expressions? There are numerous discussions in the literature, mainly based on Flory's and Huggins' original derivations. As the full treatment lies outside our scope, we here present only a simplified view, which nevertheless may aid in providing a basic understanding. The view emanates from a **molecular** or **mean field** description. We consider the actual system of interpenetrating interacting chains, which comprise the fluid mixture as being equivalent to a system of independent chains that interact with a common uniform mean field set up by the many chain system as a whole. The interaction of a given chain with all other chains, as represented in an integral form by the mean field, has two effects. The first one was discussed earlier: The contacts with other chains screen the intramolecular excluded volume interactions, thus leading to ideal chain behavior. The Flory–Huggins treatment assumes that this effect is maintained in a mixture, with unchanged conformational distributions. The second effect was already mentioned in the introduction to this chapter. Being in contact with a large number of other chains, a given chain in a binary mixture effectively integrates over the varying monomer–monomer interactions and thus probes their average value. The change in the monomer–monomer interactions following from a mixing may therefore be expressed as change of the mean field, with uniform values for all units of the A-chains and B-chains, respectively.

Equations (4.5) and (4.6) are in agreement with this picture, as can be easily verified. In order to formulate the increase in the translational entropy for $\tilde{n}_\mathrm{A}$ moles of independent A-chains, expanding from an initial volume $\mathcal{V}_\mathrm{A}$ to a final volume $\mathcal{V}$, and $\tilde{n}_\mathrm{B}$ moles of B-chains, expanding from $\mathcal{V}_\mathrm{B}$ to $\mathcal{V}$, we may just apply the standard equations used for perfect gases, and these lead exactly to Eq. (4.5). As the single chain conformational distributions should not change on mixing, we have no further contribution to the entropy (Flory addressed in his original treatment Eq. (4.5) correspondingly as the change in the total configurational entropy, rather than associating it with the center of mass motions only).

Regarding the expression for $\Delta\mathcal{G}_\mathrm{loc}$, we may first note that Eq. (4.6) represents the simplest formula which fulfills the requirement that $\Delta\mathcal{G}_\mathrm{loc}$ must vanish for $\phi_\mathrm{A} \to 0$ and $\phi_\mathrm{B} \to 0$. More about the background may be learned if we consider the change in the interaction energy following from a transfer of an A-chain from the separated state into the mixture. Each chain probes the average value of the varying contact energies with the adjacent foreign monomers, and the increase in the potential energy per reference unit may be written as

$$\frac{z_\mathrm{eff}}{2}\phi_\mathrm{B} kT\chi' \; .$$

Here, the effective coordination number z_eff gives the number of nearest neighbors (in reference units) on other chains, and a division by 2 is necessary to avoid a double count of the pair contacts. An increase in the local Gibbs free energy only results if an AB-pair is formed and this occurs with a probability

equal to the volume fraction of the B's, ϕ_{B}. The product $kT\chi'$ is meant to specify this energy increase by employing a dimensionless parameter χ'. For the potential experienced by the units of the B-chains in the mixture we write correspondingly

$$\frac{z_{\mathrm{eff}}}{2}\phi_{\mathrm{A}}kT\chi'$$

with the identical parameter χ'. To obtain $\Delta\mathcal{G}_{\mathrm{loc}}$, which refers to the total system, we have to add the contributions of all A-chains and B-chains, weighted according to the respective fraction. This leads us to

$$\begin{aligned}\Delta\mathcal{G}_{\mathrm{loc}} &= \frac{\mathcal{V}}{\tilde{v}_{\mathrm{c}}}\mathrm{N_L}\frac{z_{\mathrm{eff}}}{2}(\phi_{\mathrm{A}}\phi_{\mathrm{B}}+\phi_{\mathrm{B}}\phi_{\mathrm{A}})kT\chi' \\ &= \tilde{R}T\frac{\mathcal{V}}{\tilde{v}_{\mathrm{c}}}\phi_{\mathrm{A}}\phi_{\mathrm{B}}z_{\mathrm{eff}}\chi' \,. \end{aligned} \tag{4.7}$$

The prefactor $\mathcal{V}\mathrm{N_L}/\tilde{v}_{\mathrm{c}}$ gives the number of reference units in the system. As we can see, Eq. (4.7) is equivalent to Eq. (4.6) if we set

$$\chi = z_{\mathrm{eff}}\chi' \,. \tag{4.8}$$

Originally the χ-parameter was introduced to account for the contact energies only. However, its meaning can be generalized and in fact, this is necessary. Experiments indicate that $\Delta\mathcal{G}_{\mathrm{loc}}$ often includes an entropic part, so that we have in general

$$\Delta\mathcal{G}_{\mathrm{loc}} = \Delta\mathcal{H}_{\mathrm{mix}} - T\Delta\mathcal{S}_{\mathrm{loc}} \,. \tag{4.9}$$

The enthalpic part $\Delta\mathcal{H}_{\mathrm{mix}}$ shows up in the heat of mixing, which is positive for endothermal and negative for exothermal systems. As has already been mentioned, the entropic part $\Delta\mathcal{S}_{\mathrm{loc}}$ is usually due to changes in the number of available local conformations.

A particular concept employed in the original works must also be commented on, since it is still important. In the theoretical developments, Flory used a **lattice model**, constructed as drawn schematically in Fig. 4.2.

The A-units and B-units of the two polymer species both have the same volume v_{c} and occupy the cells of a regular lattice with coordination number z. It is assumed that the interaction energies are purely enthalpic and effective between nearest neighbors only. Excess contributions $kT\chi'$, which add to the interaction energies in the separated state, arise for all pairs of unlike monomers. The parameter $\chi = (z-2)\chi'$ was devised to deal with this model and therefore depends on the size of the cell. Flory evaluated this model with the tools of statistical thermodynamics. Using approximations, he arrived at Eqs. (4.5) and (4.6).

Although a modeling of a liquid polymer mixture on a lattice may at first look rather artificial, it makes sense because it retains the important aspects of both the entropic and enthalpic parts of $\Delta\mathcal{G}_{\mathrm{mix}}$. In recent years, lattice

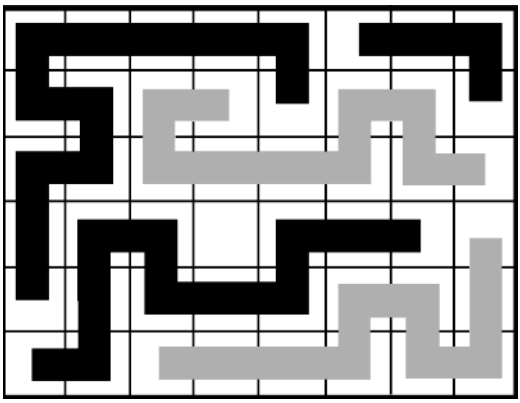

Fig. 4.2. Lattice model of a polymer mixture. Structure units of equal size setting up the two species of polymers occupy a regular lattice

models have gained a renewed importance as a concept that is suitable for computer simulations. Numerical investigations make it possible to check and assess the validity range of the Flory–Huggins treatment. In fact, limitations exist and, as analytical calculations are difficult, simulations are very helpful and important. We shall present one example in a later section.

Application of the two expressions for $\Delta\mathcal{S}_\mathrm{t}$ and $\Delta\mathcal{G}_\mathrm{loc}$, Eqs. (4.5) and (4.6), results in the Flory–Huggins formulation for the Gibbs free energy of mixing of polymer blends

$$\Delta\mathcal{G}_\mathrm{mix} = \tilde{R}T(\tilde{n}_\mathrm{A}\ln\phi_\mathrm{A} + \tilde{n}_\mathrm{B}\ln\phi_\mathrm{B} + \tilde{n}_\mathrm{c}\phi_\mathrm{A}\phi_\mathrm{B}\chi) \tag{4.10}$$

$$= \tilde{R}T\mathcal{V}\left(\frac{\phi_\mathrm{A}}{\tilde{v}_\mathrm{A}}\ln\phi_\mathrm{A} + \frac{\phi_\mathrm{B}}{\tilde{v}_\mathrm{B}}\ln\phi_\mathrm{B} + \frac{\chi}{\tilde{v}_\mathrm{c}}\phi_\mathrm{A}\phi_\mathrm{B}\right) \tag{4.11}$$

$$= \tilde{R}T\tilde{n}_\mathrm{c}\left(\frac{\phi_\mathrm{A}}{N_\mathrm{A}}\ln\phi_\mathrm{A} + \frac{\phi_\mathrm{B}}{N_\mathrm{B}}\ln\phi_\mathrm{B} + \chi\phi_\mathrm{A}\phi_\mathrm{B}\right) . \tag{4.12}$$

Here, we have introduced the molar volumes of the polymers, $\tilde{v}_\mathrm{A}$ and $\tilde{v}_\mathrm{B}$, using

$$\tilde{n}_\mathrm{A} = \mathcal{V}\frac{\phi_\mathrm{A}}{\tilde{v}_\mathrm{A}} \quad \text{and} \quad \tilde{n}_\mathrm{B} = \mathcal{V}\frac{\phi_\mathrm{B}}{\tilde{v}_\mathrm{B}} , \tag{4.13}$$

and the molar number of the reference units

$$\tilde{n}_\mathrm{c} = \frac{\mathcal{V}}{\tilde{v}_\mathrm{c}} . \tag{4.14}$$

The second equation follows when we replace the molar volumes by the degrees of polymerization expressed in terms of the numbers of structure units. If we choose the same volume, equal to the reference volume $\tilde{v}_\mathrm{c}$, for both the A-structure and B-structure units we have

$$N_\mathrm{A} = \frac{\tilde{v}_\mathrm{A}}{\tilde{v}_\mathrm{c}} \quad \text{and} \quad N_\mathrm{B} = \frac{\tilde{v}_\mathrm{B}}{\tilde{v}_\mathrm{c}} . \tag{4.15}$$

ϕ_A and ϕ_B add up to unity,

$$\phi_A + \phi_B = 1 \,. \tag{4.16}$$

The **Flory–Huggins equation** (4.11) or (4.12) is famous and widely used. It sets the basis from which the majority of discussions of the properties of polymer mixtures emanates.

Starting from $\Delta\mathcal{G}_{mix}$, the entropy of mixing, $\Delta\mathcal{S}_{mix}$, follows as

$$\begin{aligned}\Delta\mathcal{S}_{mix} &= -\frac{\partial\Delta\mathcal{G}_{mix}}{\partial T} \\ &= -\tilde{R}\mathcal{V}\left(\frac{\phi_A}{\tilde{v}_A}\ln\phi_A + \frac{\phi_B}{\tilde{v}_B}\ln\phi_B + \frac{\phi_A\phi_B}{\tilde{v}_c}\frac{\partial(\chi T)}{\partial T}\right)\end{aligned} \tag{4.17}$$

and the enthalpy of mixing, $\Delta\mathcal{H}_{mix}$, as

$$\Delta\mathcal{H}_{mix} = \Delta\mathcal{G}_{mix} + T\Delta\mathcal{S}_{mix} = \tilde{R}T\frac{\mathcal{V}}{\tilde{v}_c}\phi_A\phi_B\left(\chi - \frac{\partial(\chi T)}{\partial T}\right) \,. \tag{4.18}$$

These expressions show that the χ-parameter includes an entropic contribution given by

$$\chi_{\mathcal{S}} = \frac{\partial}{\partial T}(\chi T) \tag{4.19}$$

and an enthalpic part

$$\chi_{\mathcal{H}} = \chi - \frac{\partial(\chi T)}{\partial T} = -T\frac{\partial\chi}{\partial T} \,, \tag{4.20}$$

both setting up χ as

$$\chi = \chi_{\mathcal{H}} + \chi_{\mathcal{S}} \,. \tag{4.21}$$

Equation (4.19) indicates that for purely enthalpic local interactions, χ must have a temperature dependence

$$\chi \propto \frac{1}{T} \,. \tag{4.22}$$

In this case, the increase in entropy is associated with the translational entropy only,

$$\Delta\mathcal{S}_{mix} = \Delta\mathcal{S}_t \,, \tag{4.23}$$

and the heat of mixing is given by

$$\Delta\mathcal{H}_{mix} = \tilde{R}T\frac{\mathcal{V}}{\tilde{v}_c}\chi\phi_A\phi_B = \tilde{R}T\tilde{n}_c\chi\phi_A\phi_B \,. \tag{4.24}$$

The Flory–Huggins equation provides the basis for a general discussion of the miscibility properties of a pair of polymers. As we shall see, this can be achieved in a transparent manner and leads to clear conclusions. To start with, we recall that as a necessary requirement mixing must be accompanied

by a decrease of the Gibbs free energy. For liquid mixtures of low molar mass molecules this is mainly achieved by the large increase in the translational entropy. For these systems the increase in ΔS_t can accomplish miscibility even in the case of unfavorable AB-interaction energies, i.e., for mixtures with an endothermal heat of mixing. In polymers we find a qualitatively different situation. The Flory–Huggins equation teaches us that for polymer mixtures the increase in the translational entropy $\Delta\mathcal{S}_\mathrm{t}$ is extremely small and vanishes in the limit of infinite molar mass, i.e., $\tilde{v}_\mathrm{A}, \tilde{v}_\mathrm{B} \to \infty$. The consequences are obvious:

- Positive values of χ necessarily lead to incompatibility. Since the entropic part, $\chi_\mathcal{S}$, appears to be mostly positive, one may also state that no polymer mixtures exist with a positive heat of mixing.
- If the χ-parameter is negative, then mixing takes place.

The reason for this behavior becomes clear if we regard miscibility as the result of a competition between the osmotic pressure emerging from the translational motion of the polymers and the forces acting between the monomers. The osmotic pressure, which always favors miscibility, depends on the polymer density c_p, whereas the change in the free energy density associated with the interactions between unlike monomers – it can be positive or negative – is a function of the monomer density c_m. Since $c_\mathrm{p}/c_\mathrm{m} = 1/N$, the osmotic pressure part is extremely small compared to the effect of the monomer–monomer interactions. Hence, mutual compatibility of two polymers, i.e., their potential to form a homogeneous mixture, is almost exclusively determined by the local interactions. Endothermal conditions are the rule between two different polymers, exothermal conditions are the exception. Hence, the majority of pairs of polymers cannot form homogeneous mixtures. Compatibility is only found if there are special interactions between the A-monomers and the B-monomers as they may arise in the form of dipole–dipole forces, hydrogen bonds or special donor–acceptor interactions.

All these conclusions refer to the limit of large degrees of polymerization. It is important to see that the Flory–Huggins equation permits one to consider how the compatibility changes if the degrees of polymerization are reduced and become moderate or small. For the sake of simplicity, for a discussion we choose the case of a symmetric mixture with equal degrees of polymerization for both components, i.e.,

$$N_\mathrm{A} = N_\mathrm{B} = N \tag{4.25}$$

Using

$$\frac{\tilde{n}_\mathrm{c}}{N} = \tilde{n}_\mathrm{A} + \tilde{n}_\mathrm{B} \tag{4.26}$$

we obtain

$$\Delta\mathcal{G}_\mathrm{mix} = \tilde{R}T(\tilde{n}_\mathrm{A} + \tilde{n}_\mathrm{B})(\phi_\mathrm{A} \ln \phi_\mathrm{A} + \phi_\mathrm{B} \ln \phi_\mathrm{B} + \chi N \phi_\mathrm{A} \phi_\mathrm{B}) \; . \tag{4.27}$$

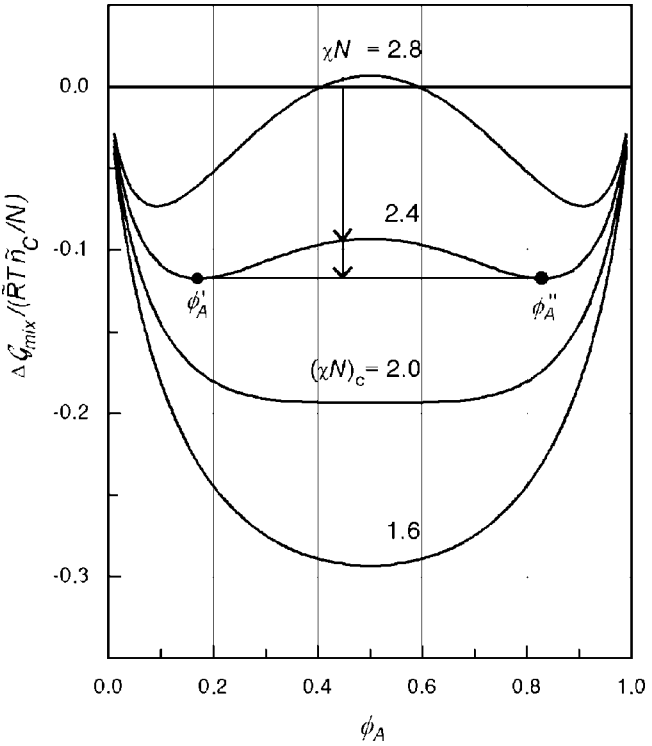

Fig. 4.3. Gibbs free energy of mixing of a symmetric binary polymer mixture ($N_\mathrm{A} = N_\mathrm{B} = N$), as described by the Flory–Huggins equation

Note that there is only one relevant parameter, namely the product $N\chi$. The dependence of $\Delta\mathcal{G}_\mathrm{mix}$ on ϕ_A is shown in Fig. 4.3, as computed for different values of χN.

A discussion of these curves enables us to reach some direct conclusions. For vanishing χ, one has negative values of $\Delta\mathcal{G}_\mathrm{mix}$ for all ϕ_A, with a minimum at $\phi_\mathrm{A} = 0.5$. In this case, we have perfect miscibility caused by the small entropic forces related with $\Delta\mathcal{S}_\mathrm{t}$. For negative values of χN, we have a further decrease of $\Delta\mathcal{G}_\mathrm{mix}$ and therefore also perfect miscibility.

A change in behavior is observed for positive values of χN. The curves alter their shape and for parameters χN above a critical value

$$(\chi N) > (\chi N)_\mathrm{c}$$

a maximum rather than a minimum emerges at $\phi_\mathrm{A} = 0.5$. This change leads us into a different situation. Even if $\Delta\mathcal{G}_\mathrm{mix}$ is always negative, there a homogeneous mixture does not always form. To understand the new conditions consider, for example, the curve for $\chi N = 2.4$ and a blend with $\phi_\mathrm{A} = 0.45$. There the two arrows are drawn. The first arrow indicates that a homogeneous mixing of A and B would lead to a decrease in the Gibbs free energy,

when compared to two separate one component phases. However, as shown by the second arrow, the Gibbs free energy can be further reduced, if again a two-phase structure is formed, now being composed of two mixed phases, with compositions ϕ'_{A} and ϕ''_{A}. The specific feature in the selected curve responsible for this peculiar behavior is the occurrence of the two minima at ϕ'_{A} and ϕ''_{A}, as these enable the further decrease of the Gibbs free energy. For which values of ϕ_{A} can this decrease be achieved? Not for all values, because there is an obvious restriction: The overall volume fraction of the A-chains has to be in the range

$$\phi'_{\mathrm{A}} \leq \phi_{\mathrm{A}} \leq \phi''_{\mathrm{A}} \, .$$

Outside this central range, for $\phi_{\mathrm{A}} < \phi'_{\mathrm{A}}$ and $\phi_{\mathrm{A}} > \phi''_{\mathrm{A}}$, a separation into the two-phases with the minimum Gibbs free energies is impossible and one homogeneous phase is formed. For a given ϕ_{A} we can calculate the fractions ϕ_1, ϕ_2 of the two coexisting mixed phases. As we have

$$\phi_{\mathrm{A}} = \phi_1 \cdot \phi'_{\mathrm{A}} + (1 - \phi_1)\phi''_{\mathrm{A}} \, , \tag{4.28}$$

we find

$$\phi_1 = \frac{\phi''_{\mathrm{A}} - \phi_{\mathrm{A}}}{\phi''_{\mathrm{A}} - \phi'_{\mathrm{A}}} \tag{4.29}$$

and

$$\phi_2 = 1 - \phi_1 = \frac{\phi_{\mathrm{A}} - \phi'_{\mathrm{A}}}{\phi''_{\mathrm{A}} - \phi'_{\mathrm{A}}} \, . \tag{4.30}$$

Hence in conclusion, for curves $\Delta\mathcal{G}_{\mathrm{mix}}(\phi_{\mathrm{A}})$, which exhibit two minima and a maximum in-between, mixing properties depend on the value of ϕ_{A}. Miscibility is found for low and high values of ϕ_{A} only, and in the central region there is a **miscibility gap**.

One can determine the critical value of χN that separates the range of perfect mixing, i.e., compatibility through all compositions, from the range with a miscibility gap. Clearly, for the critical value of χN, the curvature at $\phi_{\mathrm{A}} = 0.5$ must vanish,

$$\frac{\partial^2 \Delta\mathcal{G}_{\mathrm{mix}}(\phi_{\mathrm{A}} = 0.5)}{\partial \phi_{\mathrm{A}}^2} = 0 \, . \tag{4.31}$$

The first derivative of $\Delta\mathcal{G}_{\mathrm{mix}}$ is given by

$$\frac{1}{(\tilde{n}_{\mathrm{A}} + \tilde{n}_{\mathrm{B}})\tilde{R}T} \frac{\partial \Delta\mathcal{G}_{\mathrm{mix}}}{\partial \phi_{\mathrm{A}}} = \ln \phi_{\mathrm{A}} + 1 - \ln(1 - \phi_{\mathrm{A}}) - 1 + \chi N(1 - 2\phi_{\mathrm{A}}) \tag{4.32}$$

and the second derivative by

$$\frac{1}{(\tilde{n}_{\mathrm{A}} + \tilde{n}_{\mathrm{B}})\tilde{R}T} \frac{\partial^2 \Delta\mathcal{G}_{\mathrm{mix}}}{\partial \phi_{\mathrm{A}}^2} = \frac{1}{\phi_{\mathrm{A}}} + \frac{1}{1 - \phi_{\mathrm{A}}} - 2\chi N \, . \tag{4.33}$$

The critical value is

$$\chi N = 2 \,. \tag{4.34}$$

Hence, we expect full compatibility for

$$\chi < \chi_{\mathrm{c}} = \frac{2}{N} \tag{4.35}$$

and a miscibility gap for

$$\chi > \chi_{\mathrm{c}} \,. \tag{4.36}$$

Equations (4.35) and (4.36) describe the effect of the molar mass on the compatibility of a pair of polymers. In the limit $N \to \infty$ we have

$$\chi_{\mathrm{c}} \to 0 \,.$$

This agrees with our previous conclusion that for positive values of χ polymers of average and high molar mass do not mix at all.

The properties of symmetric polymer mixtures are summarized in the phase diagram shown in Fig. 4.4. It depicts the two regions associated with homogeneous and two-phase structures in a plot that uses the sample composition as expressed by the volume fraction ϕ_{A} and the parameter χN as variables. The boundary between the one phase and the two-phase region is called **binodal**. It is determined by the compositions ϕ'_{A} and ϕ''_{A} of the equi-

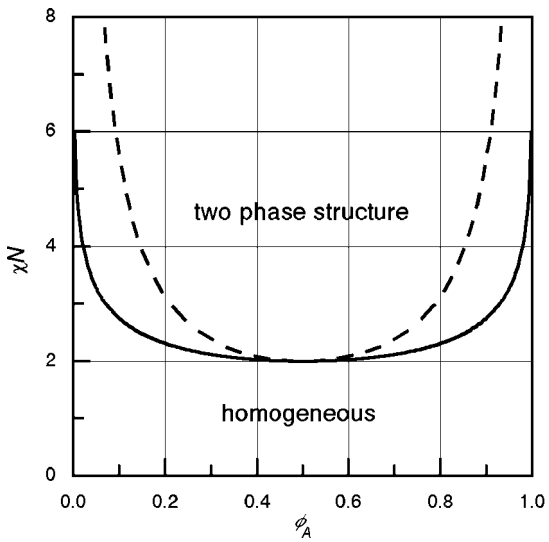

Fig. 4.4. Phase diagram of a symmetric polymer mixture ($N_{\mathrm{A}} = N_{\mathrm{B}} = N$). In addition to the binodal (*continuous line*) the spinodal is shown (*broken line*)

librium phases with minimum Gibbs free energies in the miscibility gap. ϕ'_{A} and ϕ''_{A} follow for a given value of χN from

$$\frac{\partial \Delta \mathcal{G}_{\mathrm{mix}}}{\partial \phi_{\mathrm{A}}} = 0 \; . \tag{4.37}$$

Using Eq. (4.32) we obtain an analytical expression for the binodal:

$$\chi N = \frac{1}{1-2\phi_{\mathrm{A}}} \ln \frac{1-\phi_{\mathrm{A}}}{\phi_{\mathrm{A}}} \; . \tag{4.38}$$

The derived phase diagram is universal in the sense that it is valid for all symmetric polymer mixtures. It indicates a miscibility gap for $\chi N > 2$ and enables us to make a determination of χN in this range if the compositions of the two coexisting phases are known.

For mixtures of polymers with different degrees of polymerization, i.e., $N_{\mathrm{A}} \neq N_{\mathrm{B}}$, the phase diagram loses its symmetrical shape. Figure 4.5 depicts $\Delta \mathcal{G}_{\mathrm{mix}}(\phi_{\mathrm{A}})$ for a mixture with $N_{\mathrm{B}} = 4N_{\mathrm{A}}$, as computed on the basis of the Flory–Huggins equation. Straightforward analysis shows that, in this general case, the critical value of χ is given by

$$\chi_{\mathrm{c}} = \frac{1}{2} \left(\frac{1}{\sqrt{N_{\mathrm{A}}}} + \frac{1}{\sqrt{N_{\mathrm{B}}}} \right)^2 \; . \tag{4.39}$$

The critical point where the miscibility gap begins is located at

$$\phi_{\mathrm{A,c}} = \frac{\sqrt{N_{\mathrm{B}}}}{\sqrt{N_{\mathrm{A}}} + \sqrt{N_{\mathrm{B}}}} \; . \tag{4.40}$$

The points along the binodal can be determined by the construction of the common tangent as indicated in the figure. The explanation for this procedure is simple. We refer here to the two arrows drawn at $\phi_{\mathrm{A}} = 0.45$ and the curve calculated for $\chi N_{\mathrm{A}} = 1.550$. First, consider the change in $\Delta \mathcal{G}_{\mathrm{mix}}$ if starting-off from separate states, two arbitrary mixed phases with composition ϕ^*_{A} and ϕ^{**}_{A} are formed. $\Delta \mathcal{G}_{\mathrm{mix}}$ is given by the point at $\phi_{\mathrm{A}} = 0.45$ on the straight line that connects $\Delta \mathcal{G}_{\mathrm{mix}}(\phi^*_{\mathrm{A}})$ and $\Delta \mathcal{G}_{\mathrm{mix}}(\phi^{**}_{\mathrm{A}})$. This is seen when we first write down the obvious linear relation

$$\Delta \mathcal{G}_{\mathrm{mix}}(\phi_{\mathrm{A}}) = \phi_1 \Delta \mathcal{G}_{\mathrm{mix}}(\phi^*_{\mathrm{A}}) + \phi_2 \Delta \mathcal{G}_{\mathrm{mix}}(\phi^{**}_{\mathrm{A}}) \; , \tag{4.41}$$

where ϕ_1 and ϕ_2 denote the volume fractions of the two mixed phases. Recalling that ϕ_1 and ϕ_2 are given by Eqs. (4.29) and (4.30), we obtain the expression

$$\Delta \mathcal{G}_{\mathrm{mix}}(\phi_{\mathrm{A}}) = \frac{\phi^{**}_{\mathrm{A}} - \phi_{\mathrm{A}}}{\phi^{**}_{\mathrm{A}} - \phi^*_{\mathrm{A}}} \Delta \mathcal{G}_{\mathrm{mix}}(\phi^*_{\mathrm{A}}) + \frac{\phi_{\mathrm{A}} - \phi^*_{\mathrm{A}}}{\phi^{**}_{\mathrm{A}} - \phi^*_{\mathrm{A}}} \Delta \mathcal{G}_{\mathrm{mix}}(\phi^{**}_{\mathrm{A}}) \; , \tag{4.42}$$

which indeed describes a straight line connecting $\Delta \mathcal{G}_{\mathrm{mix}}(\phi^*_{\mathrm{A}})$ and $\Delta \mathcal{G}_{\mathrm{mix}}(\phi^{**}_{\mathrm{A}})$. So far, the choice of ϕ^*_{A} and ϕ^{**}_{A} has been arbitrary, but we know that on

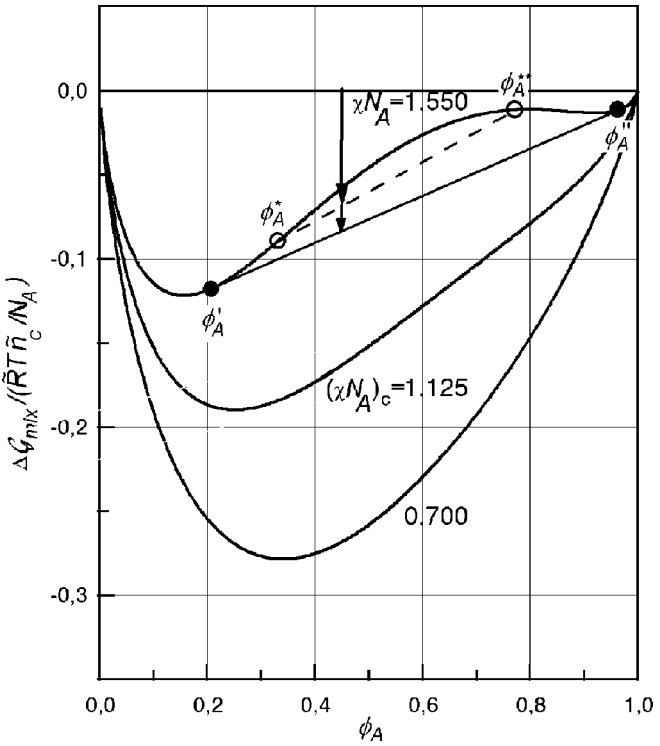

Fig. 4.5. Gibbs free energy of mixing of an asymmetric polymer mixture with $N_\mathrm{B} = 4N_\mathrm{A}$, calculated for the indicated values of χN_A. The points of contact with the common tangent, located at ϕ'_A and ϕ''_A, determine the compositions of the equilibrium phases on the binodal. The critical values are $(\chi N_\mathrm{A})_\mathrm{c} = 9/8$ and $\phi_\mathrm{c} = 2/3$

separating into two mixed phases, the system seeks to maximize the gain in Gibbs free energy. The common tangent represents that connecting line between any pair of points on the curve which is at the lowest possible level. A transition to this line therefore gives the largest possible change $\Delta\mathcal{G}_\mathrm{mix}$. It is associated with the formation of two phases with compositions ϕ'_A and ϕ''_A, as given by the points of contact with the common tangent. The binodal is set up by these points and a determination may be based on the described geometrical procedure.

4.1.1 Phase Diagrams: Upper and Lower Miscibility Gap

Phase diagrams of polymer blends under atmospheric pressure are usually presented in terms of the variables ϕ_A and T. Emanating from the discussed universal phase diagram in terms of χ and ϕ_A these can be obtained by introducing the temperature dependence of the Flory–Huggins parameter into the consideration. This function $\chi(T)$ then solely determines the appearance. For

different types of temperature dependencies $\chi(T)$, different classes of phase diagrams emerge and we shall discuss them in this section.

Let us first consider an endothermal polymer mixture with negligible entropic contributions to the local Gibbs free energy, i.e., a system with $\chi = \chi_H > 0$. Here the temperature dependence of χ is given by Eq. (4.22)

$$\chi \propto \frac{1}{T} .$$

The consequences for the phase behavior are evident. Perfect miscibility can principally exist at high temperatures, provided that the molar mass of the components are low enough. The increase of χ with decreasing temperature necessarily results in a termination of this region and the formation of a miscibility gap, found when $\chi > \chi_c$. For a symmetric mixture we obtained $\chi_c = 2/N$ (Eq. (4.36)). If χ_c is reached at a temperature T_c, we can write

$$\chi = \frac{2}{N}\frac{T_c}{T} . \tag{4.43}$$

The resulting phase diagram is shown in Fig. 4.6, together with the temperature dependence of χ. The binodal follows from Eq. (4.38), as

$$\frac{T}{T_c} = \frac{2(1-2\phi_A)}{\ln\left((1-\phi_A)/\phi_A\right)} . \tag{4.44}$$

It marks the boundary between the homogeneous state at high temperatures and the two-phase region at low temperatures.

Upon cooling a homogeneous mixture, phase separation at first sets in for samples with the **critical composition**, $\phi_A = 0.5$, at the temperature T_c. For the other samples demixing occurs at lower temperatures, as described by the binodal. We observe here a **lower miscibility gap**. A second name is also

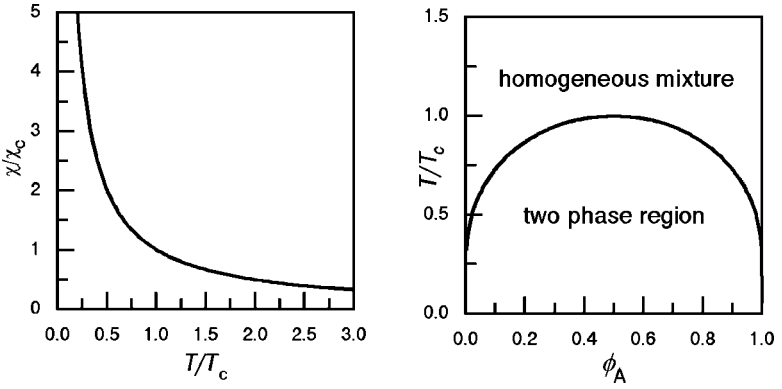

Fig. 4.6. Endothermal symmetrical mixture with a constant heat of mixing. Temperature dependence of the Flory–Huggins parameter (*left*) and phase diagram showing a lower miscibility gap (*right*)

used in the literature: T_c is called the **upper critical dissolution temperature**, shortly abbreviated UCDT. The latter name refers to the structural changes induced when coming from the two-phase region, where one observes a dissolution and merging of the two phases.

Experiments show that exothermal polymer blends sometimes have an **upper miscibility gap**, i.e., one which is open towards high temperatures. One may wonder why a mixture that is homogeneous at ambient temperature separates in two phases upon heating, and we shall have to think about possible physical mechanisms. At first, however, we discuss the formal prerequisites. On the right-hand side of Fig. 4.7 there are phase diagrams of symmetric polymer mixtures that display an upper miscibility gap. The various depicted binodals are associated with different molar mass. The curved binodals relate to polymers with low or moderate molar masses. For high molar mass, the phase boundary becomes a horizontal line and phase separation then occurs for $\chi \geq 0$ independent of ϕ_A. The latter result agrees with the general criterion for phase separations in polymer systems with high molar masses. It is therefore not particular to the symmetric system, but would be obtained in the general case, $N_A \neq N_B$, as well.

The temperature dependencies $\chi(T)$ that lead to these diagrams are shown on the left-hand side of Fig. 4.7. Their main common property is a change of the Flory–Huggins parameter from negative to positive values. The crossing of the zero line takes place at a certain temperature, denoted T_0. Coming from low temperatures, unmixing sets in for $T = T_c$ with

$$N\chi(T_c) = 2\ .$$

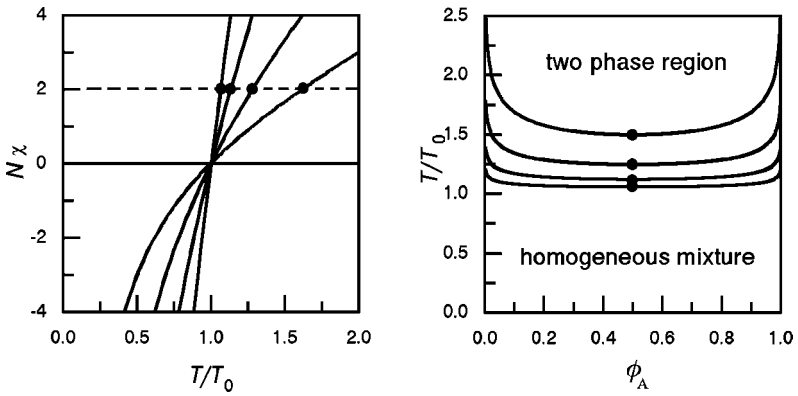

Fig. 4.7. Phase diagram of an exothermal symmetric polymer mixture with an upper miscibility gap. The binodals correspond to the different functions $N\chi(T)$ shown *on the left*, associated with an increase in the molar mass by factors 2, 4 and 8. Critical points are determined by $N\chi(T_c/T_0) = 2$, as indicated by the *filled points* in the drawings

In the limit of high degrees of polymerization we have $\chi(T_c) \to 0$ and therefore $T_c \to T_0$. We see that the prerequisite for an upper miscibility gap, or a **lower critical solution temperature**, abbreviated as LCST, as it is alternatively called, is a negative value of χ at low temperatures, followed by an increase to values above zero.

One can envisage two different mechanisms as possible explanations for such a behavior. First, there can be a competition between attractive forces between specific groups incorporated in the two polymers on one side and repulsive interactions between the remaining units on the other side. In copolymer systems with pairs of specific comonomers that are capable of forming stable bonds these conditions may arise. With increasing temperature the fraction of closed bonds decreases and the repulsive forces finally dominate. For such a system, χ may indeed be negative for low temperatures and positive for high ones.

The second conceivable mechanism has already been mentioned. Sometimes it is observed that a homogeneous mixing of two polymers results in a volume shrinkage. The related decrease in the free volume available for local motions of the monomers may lead to a reduced number of available conformations and hence a lowering of the entropy. The effect usually increases with temperature and finally overcompensates the initially dominating attractive interactions.

For mixtures of polymers with low molar mass there is also the possibility that both a lower and an upper miscibility gap appear. In this case, χ crosses the critical value χ_c twice, first during a decrease in the low temperature range and then, after passing through a minimum, during the subsequent increase at higher temperatures. Such a temperature dependence reflects the presence of both a decreasing endothermal contribution and an increasing entropic part.

As we can see, the Flory–Huggins treatment is able to account for the various general shapes of existing phase diagrams. This does not mean, however, that one can reproduce measured phase diagrams in a quantitative manner. To comply strictly with the Flory–Huggins theory, the representation of measured binodals has to be accomplished with one temperature-dependent function $\chi(T)$ only. As a matter of fact, this is rarely the case. Nevertheless, data can be formally described if one allows for a ϕ_A-dependence of χ. As long as the variations remain small, one can consider the deviations as perturbations and still feel safe on the grounds of the Flory–Huggins treatment. For some systems, however, the variations with ϕ_A are large. Then the basis is lost and the meaning of χ becomes rather unclear. Even then the Flory–Huggins equation is sometimes employed but only as a means to carry out interpolations and extrapolations and to relate different sets of data. That deviations arise is not unexpected. The mean field treatment, on which the Flory–Huggins theory is founded, is only an approximation with varying quality.

Let us look at two examples.

Figure 4.8 presents phase diagrams of mixtures of different polystyrenes with polybutadiene (PB), all of them with moderate to low molar mass

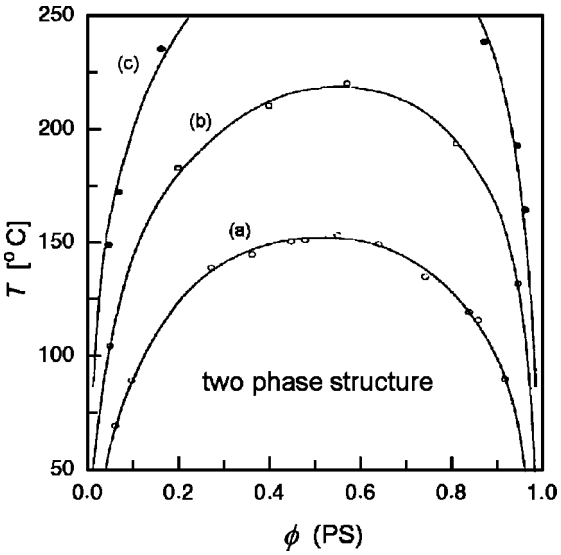

Fig. 4.8. Phase diagrams for different PS/PB-mixtures, exhibiting lower miscibility gaps. (a) $M(\mathrm{PS}) = 2250\,\mathrm{g\,mol^{-1}}$, $M(\mathrm{PB}) = 2350\,\mathrm{g\,mol^{-1}}$; (b) $M(\mathrm{PS}) = 3500\,\mathrm{g\,mol^{-1}}$, $M(\mathrm{PB}) = 2350\,\mathrm{g\,mol^{-1}}$; (c) $M(\mathrm{PS}) = 5200\,\mathrm{g\,mol^{-1}}$, $M(\mathrm{PB}) = 2350\,\mathrm{g\,mol^{-1}}$. Data from Roe and Zin [19]

($M = 2000 - 4000\,\mathrm{g\,mol^{-1}}$). The temperature points on the curves are measured **cloud points**. As samples are transparent in the homogeneous phase and become turbid when demixing starts, the cloudiness can be used for a determination of the binodal. For an accurate detection one can use measurements of the intensity of scattered or transmitted light. Here, we are dealing with an endothermal system that exhibits a lower miscibility gap. Note that T_c, as given by the highest point of each curve, decreases with decreasing molar mass in accordance with the theoretical prediction. The curves, which provide a satisfactory data fit, were obtained on the basis of the Flory–Huggins theory assuming a weakly ϕ_A-dependent χ.

As a second example, Fig. 4.9 shows a phase diagram obtained for mixtures of polystyrene and poly(vinylmethylether) (PVME). Here, one observes that homogeneous mixtures are obtained in the temperature range below 100 °C and that there is an upper miscibility gap. The phase diagram depicted in the figure was obtained for polymers with molar mass $M(\mathrm{PS}) = 2 \times 10^5\,\mathrm{g\,mol^{-1}}$, $M(\mathrm{PVME}) = 4.7 \times 10^4\,\mathrm{g\,mol^{-1}}$. For molar mass in this range the contribution of the translational entropy becomes very small indeed and mixing properties are mostly controlled by χ. The curved appearance of the binodal, which contrasts with the result of the model calculation in Fig. 4.7 where we obtained a nearly horizontal line for polymers, is indicative of a pronounced compositional dependence of χ. This represents a case where the Flory–Huggins treatment does not provide a comprehensive description. Interactions in this

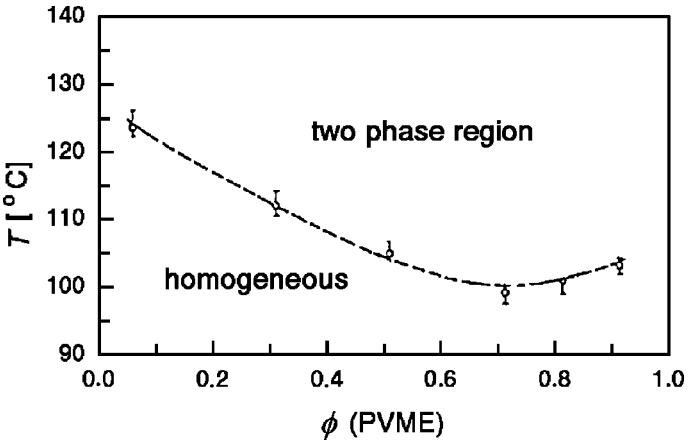

Fig. 4.9. Phase diagram of mixtures of PS ($M = 2 \times 10^5\,\mathrm{g\,mol^{-1}}$) and PVME ($M = 4.7 \times 10^4\,\mathrm{g\,mol^{-1}}$), showing an upper miscibility gap. Data from Hashimoto et al. [20]

mixture are of a complex nature and apparently change with the sample composition, so that it becomes impossible to represent them by only one constant.

4.2 Phase Separation Mechanisms

As we have seen, binary polymer mixtures can vary in structure with temperature, forming either a homogeneous phase or in a miscibility gap a two-phase structure. We now have to discuss the processes that are effective during a change, i.e., the mechanisms of phase separation.

Phase separation is induced, when a sample is transferred from the one phase region into a miscibility gap. Usually, this is accomplished by a change in temperature, upward or downward depending on the system under study. The evolution of the two-phase structure subsequent to a temperature jump can often be continuously monitored and resolved in real-time, owing to the high viscosity of polymers, which slows down the rate of unmixing. If necessary for detailed studies, the process may also be stopped at any stage by quenching samples to temperatures below the glass transition. Suitable methods for observations are light microscopy or scattering experiments.

Figure 4.10 presents as an example two micrographs obtained with a light microscope using an interference technique, showing two-phase structures observed for mixtures of polystyrene and partially brominated polystyrene ($\mathrm{PBr}_x\mathrm{S}$), with both species having equal degrees of polymerization ($N = 200$). The two components show perfect miscibility at temperatures above 220 °C and a miscibility gap below this temperature. Here phase separation was induced by a temperature jump from 230 °C to 200 °C, for two mixtures of

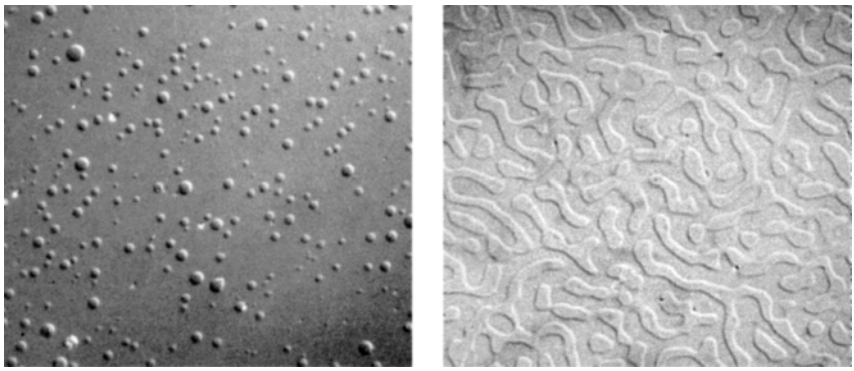

Fig. 4.10. Structure patterns emerging during phase separation in PS/PBr$_x$S-mixtures. *left*: Pattern indicating phase separation by nucleation and growth (ϕ(PS) = 0.8); *right*: Pattern suggesting phase separation by spinodal decomposition (ϕ(PS) = 0.5) [21]

different composition, ϕ(PS) = 0.8 and ϕ(PS) = 0.5. We observe two structure patterns that do not only vary in length scale, but differ in the general characteristics: The picture on the left shows spherical precipitates in a matrix, whereas the pattern on the right exhibits interpenetrating continuously extending domains. The diverse evidence suggests that different mechanisms were effective during phase separation. Structures with spherical precipitates are indicative of **nucleation and growth** and the pattern with two structurally equivalent interpenetrating phases reflects a **spinodal decomposition**. In fact, this example is quite typical and is representative of the results of investigations on various polymer mixtures. The finding is that structure evolution in the early stages of unmixing is generally controlled by either of these two mechanisms.

The cause for the occurrence of two different modes of phase separation becomes revealed when we consider the shape of the curve $\Delta\mathcal{G}_{\mathrm{mix}}(\phi_{\mathrm{A}})$. As ϕ_{A} is the only independent variable, in the following we will omit the subscript A, i.e., replace ϕ_{A} by the shorter symbol ϕ. The upper part of Fig. 4.11 depicts functions $\Delta\mathcal{G}_{\mathrm{mix}}(\phi)$ computed for three different values of χ, which belong to the one phase region (χ_{i}), the two-phase region (χ_{f}) and the critical point (χ_{c}). The lower part of the figure gives the phase diagram, with the positions of $\chi_{\mathrm{i}}, \chi_{\mathrm{f}}$ and χ_{c} being indicated. The arrows '1' and '2' indicate two jumps that transfer a polymer mixture from the homogeneous phase into the two-phase region.

Immediately after the jump, the structure is still homogeneous but, of course, no longer stable. What is different in the two cases, is the character of the instability. The difference shows up when we consider the consequences of a spontaneous local concentration fluctuation, as it could be thermally induced directly after the jump. Figure 4.12 represents such a fluctuation

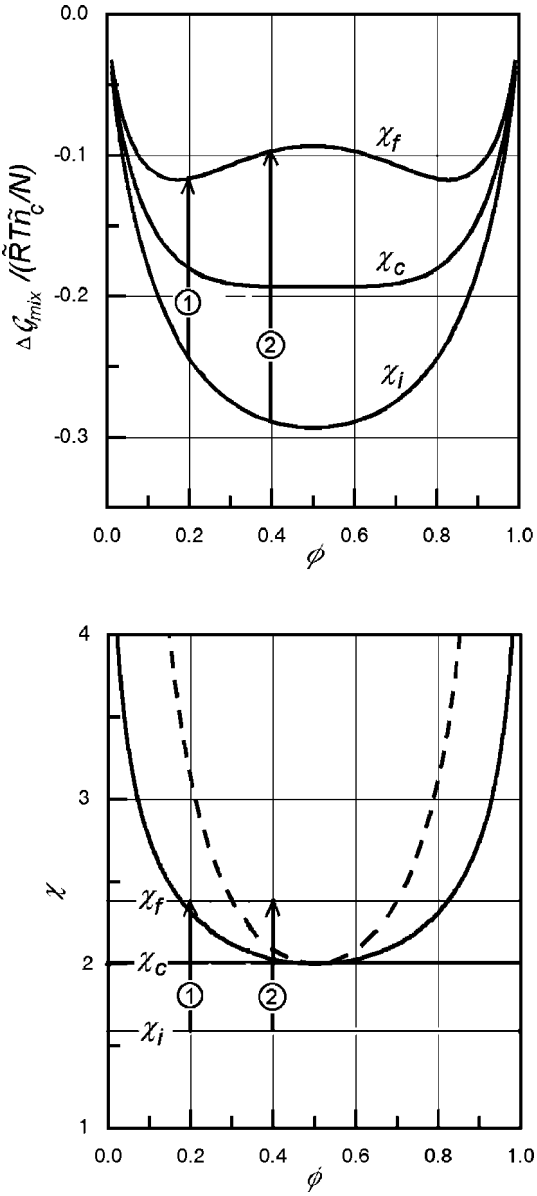

Fig. 4.11. Temperature jumps that transfer a symmetric binary polymer mixture from the homogeneous state into the two-phase region. Depending upon the location in the two-phase region, phase separation occurs either by nucleation and growth ('1') or by spinodal decomposition ('2')

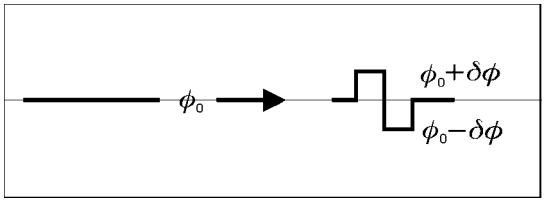

Fig. 4.12. Local concentration fluctuation

schematically, being set up by an increase $\delta\phi$ in the concentration of A-chains in one half of a small volume $\mathrm{d}^3\boldsymbol{r}$ and a corresponding decrease in the other half. The fluctuation leads to a change in the Gibbs free energy, described as

$$\delta\mathcal{G} = \frac{1}{2}(g(\phi_0+\delta\phi)+g(\phi_0-\delta\phi))\,\mathrm{d}^3\boldsymbol{r} - g(\phi_0)\,\mathrm{d}^3\boldsymbol{r}\;. \tag{4.45}$$

Here, we have introduced the free energy density, i.e., the Gibbs free energy per unit volume, denoted $g(\phi)$. Series expansion of $g(\phi)$ up to the second order in ϕ for $\delta\mathcal{G}$ yields the expression

$$\delta\mathcal{G} = \frac{1}{2}\frac{\partial^2 g}{\partial\phi^2}(\phi_0)\delta\phi^2\,\mathrm{d}^3\boldsymbol{r}\;. \tag{4.46}$$

We calculate $\partial^2 g/\partial\phi^2$ with the aid of the Flory–Huggins equation, i.e., write

$$\frac{\partial^2 g}{\partial\phi^2} = \frac{1}{\mathcal{V}}\frac{\partial^2\Delta\mathcal{G}_{\mathrm{mix}}}{\partial\phi^2} \tag{4.47}$$

with $\Delta\mathcal{G}_{\mathrm{mix}}$ given by Eq. (4.11). Then the change $\delta\mathcal{G}$ associated with the local fluctuation is

$$\delta\mathcal{G} = \frac{1}{2}\frac{1}{\mathcal{V}}\frac{\partial^2\Delta\mathcal{G}_{\mathrm{mix}}}{\partial\phi^2}(\phi_0)\delta\phi^2\,\mathrm{d}^3\boldsymbol{r}\;. \tag{4.48}$$

This is a most interesting result. It tells us that, depending on the sign of the curvature $\partial^2\Delta\mathcal{G}_{\mathrm{mix}}/\partial\phi^2$, the fluctuation may either lead to an increase, or a decrease in the Gibbs free energy. In stable states, there always has to be an increase to ensure that a spontaneous local association of monomers A disintegrates again. This situation is found for jump '1'. It leads to a situation where the structure is still stable with regard to spontaneous concentration fluctuations provided that they remain sufficiently small. Jump '2' represents a qualitatively different case. Since the curvature here is negative, the Gibbs free energy decreases immediately, even for an infinitesimally small fluctuation, and no restoring force arises. On the contrary, there is a tendency for further growth of the fluctuation amplitude. Hence, by the temperature jump '2' an initial structure is prepared, which is perfectly unstable.

It is exactly the latter situation which results in a spinodal decomposition. The process is sketched at the bottom of Fig. 4.13. The drawing indicates

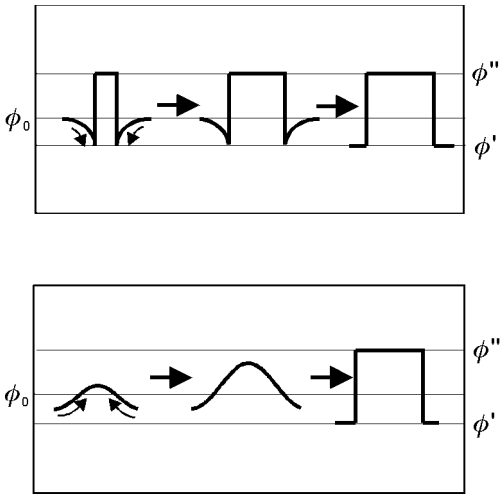

Fig. 4.13. Mechanisms of phase separation: Nucleation and growth (*top*) and spinodal decomposition (*bottom*). The *curved small arrows* indicate the direction of the diffusive motion of the A-chains

that a spinodal decomposition implies a continuous growth of the amplitude of a concentration fluctuation, starting from infinitesimal values and ensuing up to the final state of two equilibrium phases with compositions ϕ' and ϕ''. The principles governing this process have been studied in numerous investigations and clarified to a large extent. We shall discuss its properties in detail in the next section. At this point, we leave it with one short remark with reference to the figure. There the arrows indicate the directions of flow of the A-chains. The normal situation is found for nucleation and growth, where the flow is directed as usual, towards decreasing concentrations of the A-chains. In spinodal decompositions, the flow direction is reversed. The A-chains diffuse towards higher concentrations, which formally corresponds to a negative diffusion coefficient.

The upper half of the figure shows the process that starts subsequent to the temperature jump '1'. As small fluctuations decay again, the only way to achieve a gain in the Gibbs free energy is a large fluctuation, which directly leads to the formation of a nucleus of the new equilibrium phase with composition ϕ''. After it has formed it can increase in size. Growth is accomplished by regular diffusion of the chains since there exists, as indicated in the drawing, a zone with a reduced ϕ at the surface of the particle that attracts a stream of A-chains.

The process of nucleation and growth is not peculiar to polymers, but observed in many materials and we consider it only briefly. The specific point making up the difference to the case of a spinodal decomposition is the existence of an activation barrier. The reason for its occurrence is easily recog-

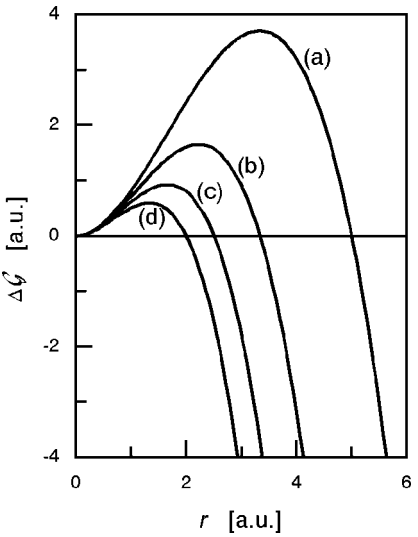

Fig. 4.14. Activation barrier encountered during formation of a spherical nucleus. Curves (a)–(d) correspond to a sequence 2:3:4:5 of values for $\Delta g/\sigma_{\mathrm{if}}$

nized. Figure 4.14 shows the change of the Gibbs free energy, $\Delta\mathcal{G}$, following from the formation of a spherical precipitate of the new equilibrium phase.

$\Delta\mathcal{G}$ depends on the radius r of the precipitate, as described by the equation

$$\Delta\mathcal{G}(r) = -\frac{4\pi}{3}r^3\Delta g + 4\pi r^2\sigma_{\mathrm{if}} \tag{4.49}$$

with

$$\Delta g = g(\phi_0) - g(\phi'') \; . \tag{4.50}$$

Equation (4.49) emanates from the view that $\Delta\mathcal{G}$ is set up by two contributions, one being related to the gain in the bulk Gibbs free energy of the precipitate, the other to the effect of the interface between particle and matrix. This interface is associated with an excess free energy and the symbol σ_{if} stands for the excess free energy per unit area.

Since the building up of the interface causes an increase in the free energy, a barrier $\Delta\mathcal{G}_{\mathrm{b}}$ develops, which first has to be overcome before growth can set in. The passage over this barrier constitutes the nucleation step. Representing an activated process, it occurs with a rate given by the Arrhenius equation,

$$\nu_{\mathrm{nuc}} \propto \exp -\frac{\Delta\mathcal{G}_{\mathrm{b}}}{kT} \; , \tag{4.51}$$

whereby $\Delta\mathcal{G}_{\mathrm{b}}$ is the barrier height

$$\Delta\mathcal{G}_{\mathrm{b}} = \frac{16\pi}{3}\frac{\sigma_{\mathrm{if}}^3}{(\Delta g)^2} \; . \tag{4.52}$$

Equation (4.52) follows from Eq. (4.49) when searching for the maximum. $\Delta\mathcal{G}_\mathrm{b}$ increases with decreasing distance from the binodal where we have $\Delta g = 0$. The change is illustrated by the curves in Fig. 4.14, which were calculated for different values of the ratio $\Delta g/\sigma_\mathrm{if}$. We learn from this behavior that, in order to achieve reasonable rates, nucleation requires a certain degree of supercooling (or overheating, if there is an upper miscibility gap).

Nucleation and growth occurs if the unmixing is induced at a temperature near the binodal, where the system is still stable with regard to small concentration fluctuations. Further away from the binodal this restricted **metastability** is lost and spinodal decomposition sets in. Transition from one growth regime to another occurs in the range of the **spinodal**, which is defined as the locus of those points in the phase diagram where the stabilizing restoring forces vanish. According to the previous arguments this occurs for

$$\frac{\partial^2 \Delta\mathcal{G}_\mathrm{mix}}{\partial\phi^2} = 0 \,. \tag{4.53}$$

Equation (4.53) determines a certain value χ for each ϕ and for the resulting spinodal curve we choose the designation $\chi_\mathrm{sp}(\phi)$. In the case of a symmetric mixture with a degree of polymerization N for both species, we can use Eq. (4.33) for a determination. The spinodal follows as

$$\chi_\mathrm{sp} = \frac{1}{2N\phi_\mathrm{A}(1-\phi_\mathrm{A})} \,. \tag{4.54}$$

It is this line that is included in Figs. 4.4 and 4.11. For $N_\mathrm{A} \neq N_\mathrm{B}$ we start from Eq. (4.11) and obtain

$$\frac{\partial^2 \Delta\mathcal{G}_\mathrm{mix}}{\partial\phi^2} \propto \frac{1}{N_\mathrm{A}\phi} + \frac{1}{N_\mathrm{B}(1-\phi)} + \frac{\partial^2}{\partial\phi^2}\chi\phi(1-\phi) \,. \tag{4.55}$$

In this case, the spinodal is given by the function

$$2\chi_\mathrm{sp} = \frac{1}{N_\mathrm{A}\phi} + \frac{1}{N_\mathrm{B}(1-\phi)} \,. \tag{4.56}$$

As was mentioned earlier, reality in polymer mixtures often differs from the Flory–Huggins model in that a ϕ-dependent χ is required. Then we have to write for the equation of the spinodal

$$\frac{1}{N_\mathrm{A}\phi} + \frac{1}{N_\mathrm{B}(1-\phi)} = -\frac{\partial^2}{\partial\phi^2}(\chi(\phi)\phi(1-\phi)) = 2\Lambda \,. \tag{4.57}$$

Here we have introduced another function, Λ, which is related to χ by

$$\Lambda = \chi - (1-2\phi)\frac{\partial\chi}{\partial\phi} - \frac{1}{2}\phi(1-\phi)\frac{\partial^2\chi}{\partial\phi^2} \,. \tag{4.58}$$

We see that the situation has now become more involved. As we shall learn in the next section, rather than χ, Λ follows from an experimental determination of the spinodal.

It might appear at first that the spinodal marks a sharp transition between two growth regimes, but this is not true. Activation barriers for the nucleation are continuously lowered when approaching the spinodal and thus may lose their effectiveness already prior to the crossing. As a consequence, the transition from the nucleation and growth regime to the region of spinodal decompositions is actually diffuse and there is no way to employ it for an accurate determination of the spinodal. There is, however, another effect for which the spinodal is significant and well-defined: The distance from the spinodal controls the concentration fluctuations in the homogeneous phase. The next section deals in detail with this interesting relationship.

4.3 Critical Fluctuations and Spinodal Decomposition

The critical point of a polymer mixture, as given by the critical temperature T_c jointly with the critical composition ϕ_c, is the locus of a **second order phase transition**. Second order phase transitions have general properties that are found independent of the particular system; this may be a ferromagnetic or ferroelectric solid near its Curie temperature, a gas near the critical point, or, as in our case, a mixture. As one general law, the approach of a critical point is always accompanied by a strong increase of the local fluctuations of the **order parameter** associated with the transition. For our mixture, the order parameter is given by the composition, as specified, for example, by the volume fraction of A-chains. So far, we have been concerned with the overall concentrations of the A- and B-chains in the sample only. On microscopic scales, concentrations are not uniform but show fluctuations about the mean value, owing to the action of random thermal forces. According to the general scenario of critical phase transitions, one expects a steep growth of these fluctuations on approaching T_c.

The most convenient technique for a verification are scattering experiments, as these probe the fluctuations directly. Figure 4.15 presents, as an example, results obtained by neutron scattering for a mixture of (deuterated) polystyrene and poly(vinylmethylether). As was mentioned earlier, this system shows an upper miscibility gap (Fig. 4.9). Measurements were carried out for a mixture with the critical composition at a series of temperatures in the one phase region. The figure depicts the reciprocals of the scattering intensities in plots versus q^2. We notice that approaching the critical point indeed leads to an overall increase of the intensities, with the strongest growth being found for the scattering in the forward direction $q \to 0$. The temperature dependence of the forward scattering is shown on the right hand side, in a plot of $S^{-1}(q \to 0)$ against $1/T$. Data indicate a divergence, and its location determines the critical temperature. Here we find $T_c = 131.8\,^{\circ}\mathrm{C}$.

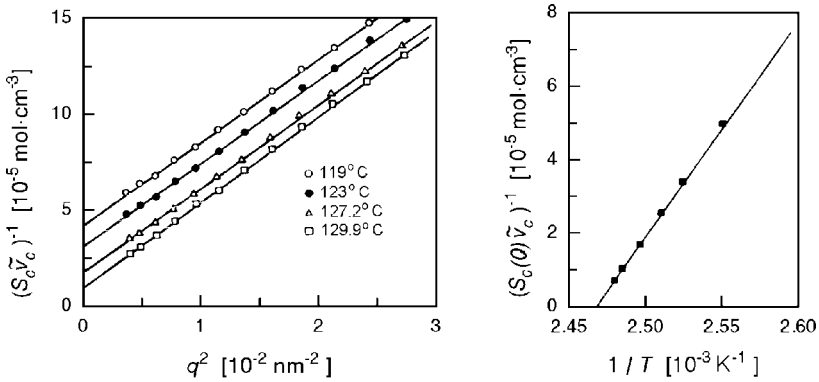

Fig. 4.15. Results of neutron scattering experiments on a (0.13:0.87)-mixture of d-PS ($M = 3.8 \times 10^5\,\mathrm{g\,mol^{-1}}$) and PVME ($M = 6.4 \times 10^4\,\mathrm{g\,mol^{-1}}$). S_c denotes the scattering function Eq. (4.79) referring to structure units with a molar volume $\tilde{v}_c$. Intensities increase on approaching the critical point (*left*). Extrapolation of $S(q \to 0)$ to the point of divergence yields the critical temperature (*right*). Data from Schwahn et al. [22]

When the phase boundary is crossed through the critical point, a spinodal decomposition is initiated, and it can be followed by time-dependent scattering experiments. Figure 4.16 shows the evolution of the scattering function during the first stages, subsequent to a rapid change from an initial temperature T_{in} two degrees below T_c, to $T_{\mathrm{fi}} = 134.1\,^{\circ}\mathrm{C}$, located $2.3\,^{\circ}\mathrm{C}$ above. Beginning at zero time with the equilibrium structure factor associated with the temperature T_{in} in the homogeneous phase, a peak emerges and grows in intensity.

Figure 4.17 presents, as a second example, a further experiment on mixtures of polystyrene and poly(vinylmethylether), now carried out by time dependent light scattering experiments (this sample had a lower critical temperature, probably due to differences in behavior between normal and deuterated polystyrene). Experiments encompass a larger time range and probe the scattering at the small q's reached when using light. Again one observes the development of a peak, and it also stays at first at a constant position. Here, we can see that during the later stages it shifts to lower scattering angles.

This appearance of a peak which grows in intensity, initially at a fixed position and then shifting to lower scattering angles, can in fact be considered as indicative of a spinodal decomposition. One can say that the peak reflects the occurrence of wave-like modulations of the local blend composition, with a dominance of particular wavelengths. Furthermore, the intensity increase indicates a continuous amplitude growth. This, indeed, is exactly the process sketched at the bottom of Fig. 4.13.

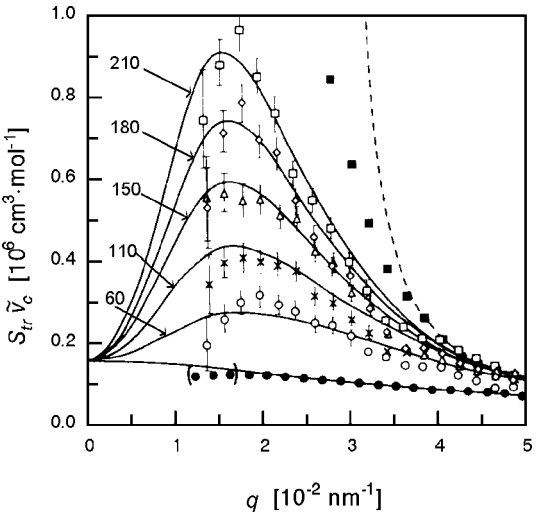

Fig. 4.16. The same system as in Fig. 4.15. Transient scattering functions $S_{\mathrm{tr}}(q,t)$ measured after a temperature jump from $T_{\mathrm{in}} = 130\,^{\circ}\mathrm{C}$ (one phase region) to $T_{\mathrm{fi}} = 134.1\,^{\circ}\mathrm{C}$ (two-phase region). Times of evolution are indicated (in seconds) [22]

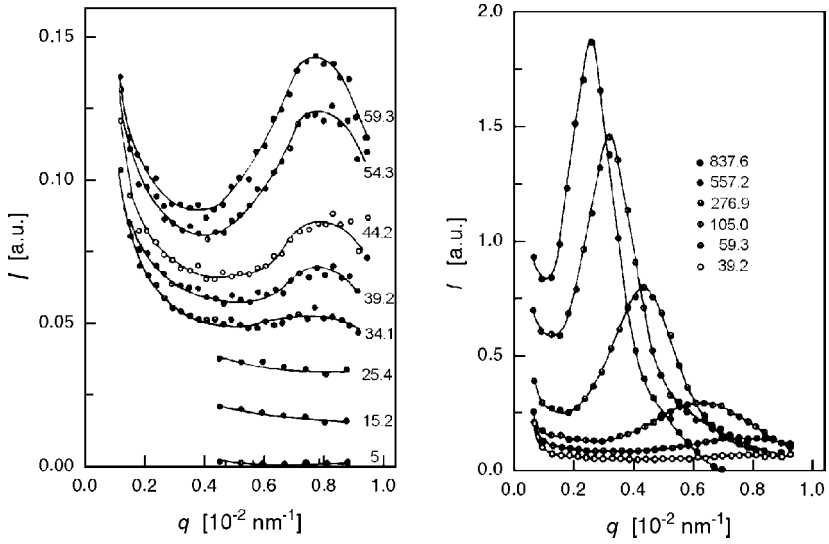

Fig. 4.17. Time dependent light scattering experiments, conducted on a (0.3:0.7)-mixture of PS ($M = 1.5 \times 10^5\,\mathrm{g\,mol^{-1}}$) and PVME ($M = 4.6 \times 10^4\,\mathrm{g\,mol^{-1}}$) subsequent to a rapid transfer from a temperature in the region of homogeneous states to the temperature $T_{\mathrm{fi}} = 101\,^{\circ}\mathrm{C}$ located in the two-phase region. Numbers give the time passed after the jump (in seconds). Data from Hashimoto et al. [23]

All these findings, the steep growth of the concentration fluctuations in the homogeneous phase near the critical point, as well as the kinetics of spinodal decomposition with its strong preference for certain wavelengths, can be treated in a common theory. It was originally developed by Cahn, Hilliard, and Cook, in order to treat unmixing phenomena in metallic alloys and anorganic glasses, and then adjusted by de Gennes and Binder to the polymer case. Polymers actually represent systems that exhibit these phenomena in a particularly clear form and thus allow a verification of the theories. In the following three subsections, which concern the critical scattering as observed in the homogeneous phase, the initial stages of spinodal decomposition and the late stage kinetics, some main results will be presented.

4.3.1 Critical Scattering

Here we consider the concentration fluctuations in the homogeneous phase and also the manner in which these are reflected in measured scattering functions.

How can one deal with the fluctuations? At first view it might appear that the Flory–Huggins treatment does not give any help. Accounting for all microscopic states, the Flory–Huggins expression for the Gibbs free energy includes also the overall effect of all the concentration fluctuations in a mixture. The overall effect, however, is not our point of concern. We wish to grasp a *single* fluctuation state, as given by a certain distribution of the A's specified by a function $\phi(\boldsymbol{r})$ and determine its statistical weight. What we need for this purpose is a knowledge about a *constrained* Gibbs free energy, namely that associated with a single fluctuation state only.

To solve our problem we use a trick that was originally employed by Kadanoff in an analysis of the critical behavior of ferromagnets. Envisage a division of the sample volume in a large number of cubic 'blocks', with volumes v_B that, although being very small, still allow the use of thermodynamic laws; block sizes in the order of 10–100 nm^3 seem appropriate for this purpose. For this grained system, the description of a certain fluctuation state is accomplished by giving the concentrations ϕ_i of all blocks i. The (constrained) free energy of a thus characterized fluctuation state can be written down, proceeding in three steps. As we may apply the Flory–Huggins equation for each block separately, we first write a sum

$$\mathcal{G}(\{\phi_i\}) = \sum_i v_\mathrm{B} g(\phi_i) \; . \tag{4.59}$$

Here, g stands for the free energy density of the mixture

$$g(\phi) = \phi g_\mathrm{A} + (1-\phi) g_\mathrm{B} + \tilde{R}T \left[\frac{\phi}{\tilde{v}_\mathrm{A}} \ln \phi + \frac{(1-\phi)}{\tilde{v}_\mathrm{B}} \ln(1-\phi) + \frac{\chi}{\tilde{v}_\mathrm{c}} \phi(1-\phi) \right] \; , \tag{4.60}$$

g_A and g_B denoting the free energy densities of the one component phases. Being in close contact, neighboring blocks, interact with each other across the interfaces and we have to inquire about the related interfacial energy. We know that it must vanish for equal concentrations and increase with the concentration difference, independent of the direction of change. The simplest expression with such properties is the quadratic term

$$\beta(\phi_i - \phi_j)^2 \ ,$$

where ϕ_i, ϕ_j are the concentrations in the adjacent blocks. It includes a coefficient β that determines the strength of the interaction. We add this term to the first sum and write

$$\mathcal{G}(\{\phi_i\}) = \sum_i v_\mathrm{B} g(\phi_i) + \sum_{ij} \beta(\phi_i - \phi_j)^2 \ . \tag{4.61}$$

Finally, replacing the summation by an integral, we obtain

$$\mathcal{G}(\phi(\boldsymbol{r})) = \int \left(g(\phi(\boldsymbol{r})) + \beta'(\nabla\phi)^2\right) \mathrm{d}^3\boldsymbol{r} \tag{4.62}$$

with $\beta' = \beta v_\mathrm{B}^{-1/3}$. With this result we have solved our problem. Equation (4.62) describes in an approximate, empirical manner the free energy to be attributed to a given fluctuation state $\phi(\boldsymbol{r})$. It is known in the literature as **Ginzburg–Landau functional** and is widely applied in treatments of various kinds of fluctuations.

The equation can be further simplified if a linearization approximation is used. Clearly the state with a uniform concentration,

$$\phi(\boldsymbol{r}) = \mathrm{const} = \phi \ ,$$

has the lowest free energy, $\mathcal{G}_\mathrm{min}$. For considering the change in the Gibbs free energy

$$\delta\mathcal{G} = \mathcal{G} - \mathcal{G}_\mathrm{min}$$

as it results from a fluctuation

$$\delta\phi(\boldsymbol{r}) = \phi(\boldsymbol{r}) - \phi$$

we may use a series expansion of $g(\delta\phi)$ up to the second order

$$\delta\mathcal{G} = \int_\mathcal{V} \left(\delta g(\delta\phi(\boldsymbol{r})) + \beta'(\nabla\delta\phi)^2\right) \mathrm{d}^3\boldsymbol{r} \tag{4.63}$$

$$= \frac{\partial g}{\partial\phi} \int_\mathcal{V} \delta\phi \mathrm{d}^3\boldsymbol{r} + \frac{1}{2}\frac{\partial^2 g}{\partial\phi^2} \int_\mathcal{V} (\delta\phi)^2 \,\mathrm{d}^3\boldsymbol{r} + \beta' \int_\mathcal{V} (\nabla\delta\phi)^2 \,\mathrm{d}^3\boldsymbol{r} \ . \tag{4.64}$$

Conservation of the masses of the two species implies

$$\int_{\mathcal{V}} \delta\phi \, \mathrm{d}^3\boldsymbol{r} = 0 \, , \tag{4.65}$$

and we only have to calculate the second derivative of g. This leads to

$$\delta\mathcal{G} = \frac{\tilde{R}T}{2} \left(\frac{1}{\tilde{v}_\mathrm{A}\phi} + \frac{1}{\tilde{v}_\mathrm{B}(1-\phi)} - \frac{2\chi}{\tilde{v}_\mathrm{c}} \right) \int_{\mathcal{V}} (\delta\phi)^2 \, \mathrm{d}^3\boldsymbol{r} + \beta' \int_{\mathcal{V}} (\nabla\delta\phi)^2 \, \mathrm{d}^3\boldsymbol{r} \, . \tag{4.66}$$

This is a useful result. It relates the Gibbs free energy of a given fluctuation state to two parameters only, namely the integral or mean values of $(\delta\phi)^2$ and $(\nabla\delta\phi)^2$.

We now turn to scattering experiments. They may generally be regarded as carrying out a Fourier analysis, in our case a Fourier analysis of the concentration fluctuations in the mixture. We therefore represent $\delta\phi(\boldsymbol{r})$ as a sum of wave-like modulations with amplitudes $\phi_{\boldsymbol{k}}$

$$\delta\phi(\boldsymbol{r}) = \mathcal{V}^{-1/2} \sum_{\boldsymbol{k}} \exp(\mathrm{i}\boldsymbol{k}\boldsymbol{r})\phi_{\boldsymbol{k}} \, . \tag{4.67}$$

For a finite sample volume $\mathcal{V}$, the sum includes a sequence of discrete values of $\boldsymbol{k}$ (see Eq. (A.117)). When writing a Fourier series in terms of exponential functions, the amplitudes $\phi_{\boldsymbol{k}}$ are complex numbers

$$\phi_{\boldsymbol{k}} = |\phi_{\boldsymbol{k}}| \exp(\mathrm{i}\varphi_{\boldsymbol{k}})$$

with a modulus $|\phi_{\boldsymbol{k}}|$ and a phase $\varphi_{\boldsymbol{k}}$. Since $\delta\phi(\boldsymbol{r})$ is a real quantity, we have

$$\phi_{-\boldsymbol{k}} = \phi_{\boldsymbol{k}}^* \tag{4.68}$$

and therefore

$$|\phi_{\boldsymbol{k}}| = |\phi_{-\boldsymbol{k}}| \, . \tag{4.69}$$

When we introduce the Fourier series into the integral of Eq. (4.66), we obtain

$$\int_{\mathcal{V}} (\delta\phi)^2 \, \mathrm{d}^3\boldsymbol{r} = \mathcal{V}^{-1} \sum_{\boldsymbol{k},\boldsymbol{k}'} \phi_{\boldsymbol{k}}\phi_{\boldsymbol{k}'} \int_{\mathcal{V}} \exp[\mathrm{i}(\boldsymbol{k}\boldsymbol{r} + \boldsymbol{k}'\boldsymbol{r})] \, \mathrm{d}^3\boldsymbol{r} \, . \tag{4.70}$$

Since

$$\int_{\mathcal{V}} \exp[\mathrm{i}(\boldsymbol{k} + \boldsymbol{k}')\boldsymbol{r}] \; \mathrm{d}^3\boldsymbol{r} = \mathcal{V}\delta_{\boldsymbol{k},-\boldsymbol{k}'} \tag{4.71}$$

we can write

$$\int_{\mathcal{V}} (\delta\phi)^2 \, \mathrm{d}^3\boldsymbol{r} = \sum_{\boldsymbol{k}} \phi_{\boldsymbol{k}}\phi_{-\boldsymbol{k}} = \sum_{\boldsymbol{k}} |\phi_{\boldsymbol{k}}|^2 \, . \tag{4.72}$$

For the gradient term we obtain in similar manner

$$\int_{\mathcal{V}} (\nabla\delta\phi)^2 \,\mathrm{d}^3\boldsymbol{r} = \sum_{\boldsymbol{k}} (\mathrm{i}\boldsymbol{k}) \cdot (-\mathrm{i}\boldsymbol{k}) \phi_{\boldsymbol{k}} \phi_{-\boldsymbol{k}} = \sum_{\boldsymbol{k}} |\boldsymbol{k}|^2 |\phi_{\boldsymbol{k}}|^2 \,. \tag{4.73}$$

Introducing Eqs. (4.72), (4.73) into Eq. (4.66), we obtain

$$\delta\mathcal{G} = \frac{\tilde{R}T}{2} \sum_{\boldsymbol{k}} \left(\frac{1}{\tilde{v}_{\mathrm{A}}\phi} + \frac{1}{\tilde{v}_{\mathrm{B}}(1-\phi)} - \frac{2\chi}{\tilde{v}_{\mathrm{c}}} + \beta''|\boldsymbol{k}|^2 \right) |\phi_{\boldsymbol{k}}|^2 \,. \tag{4.74}$$

The coupling constant $\beta'' = 2\beta'(\tilde{R}T)^{-1}$ is unknown at this point of the discussion, but later on we shall learn more about it.

As we can see, the Fourier transformation leads to a decoupling. Whereas, in direct space, we have a short-ranged coupling between fluctuations at different positions as expressed by the gradient term in Eq. (4.66), different Fourier amplitudes $\phi_{\boldsymbol{k}}$ contribute separately to $\delta\mathcal{G}$, thus being perfectly independent. Hence, the wave-like modulations of the concentration may be regarded as the basic **modes** of the system, which can be excited independently from each other. The general dynamics of the concentration fluctuations in a polymer mixture is described as a superposition of all these modes, each mode being characterized by a certain wavevector.

Having an expression for the free energy increase associated with the excitation of the mode $\boldsymbol{k}$, one can calculate its mean squared amplitude in thermal equilibrium $\langle|\phi_{\boldsymbol{k}}|^2\rangle$. It follows from Boltzmann statistics as

$$\langle|\phi_{\boldsymbol{k}}|^2\rangle = \int |\phi_{\boldsymbol{k}}|^2 \exp -\frac{\delta\mathcal{G}(\phi_{\boldsymbol{k}})}{kT} \delta|\phi_{\boldsymbol{k}}| \Big/ \int \exp -\frac{\delta\mathcal{G}(\phi_{\boldsymbol{k}})}{kT} \delta|\phi_{\boldsymbol{k}}| \,. \tag{4.75}$$

Evaluation of the integrals yields

$$\langle|\phi_{\boldsymbol{k}}|^2\rangle = {\mathrm{N_L}}^{-1} \left(\frac{1}{\tilde{v}_{\mathrm{A}}\phi} + \frac{1}{\tilde{v}_{\mathrm{B}}(1-\phi)} - \frac{2\chi}{\tilde{v}_{\mathrm{c}}} + \beta''|\boldsymbol{k}|^2 \right)^{-1} \,. \tag{4.76}$$

The result includes a singularity that comes up if the denominator equals zero. It tells us that finite concentration fluctuations can exist only under the condition

$$\frac{1}{\tilde{v}_{\mathrm{A}}\phi} + \frac{1}{\tilde{v}_{\mathrm{B}}(1-\phi)} - \frac{2\chi}{\tilde{v}_{\mathrm{c}}} + \beta''|\boldsymbol{k}|^2 > 0 \,. \tag{4.77}$$

Regarding Eq. (4.56), this is equivalent to

$$\chi_{\mathrm{sp}} - \chi + \frac{\tilde{v}_{\mathrm{c}}}{2}\beta''|\boldsymbol{k}|^2 > 0 \,. \tag{4.78}$$

As we can see, in the limit $k \to 0$, the stability criterion of the Flory–Huggins theory, $\chi < \chi_{\mathrm{sp}}$, is recovered. For finite values of k, the criterion becomes modified.

Next, we relate the calculated fluctuations amplitudes to the scattering function obtained in X-ray or light scattering experiments. Discussions are usually based on a scattering function that refers to the reference volume common for both species, v_c, or in the language of the lattice models, on a scattering function that refers to the cells of the lattice. It is denoted as S_c and defined as

$$S_c(\boldsymbol{q}) = \frac{1}{\mathcal{N}_c}\langle |C(\boldsymbol{q})|^2\rangle \ . \tag{4.79}$$

$C(\boldsymbol{q})$ is the scattering amplitude and $\mathcal{N}_c$ stands for the total number of A-units and B-units in the sample. The scattering function $S_c(\boldsymbol{q})$ can be directly related to the mean squared amplitudes of the fluctuations $\langle|\phi_{\boldsymbol{k}}|^2\rangle$. As is shown in Sect. A.4.1 in the Appendix, the relation is

$$S_c(\boldsymbol{q}) = \frac{1}{v_c}\langle |\phi_{\boldsymbol{k}=\boldsymbol{q}}|^2\rangle \ . \tag{4.80}$$

Making use of Eq. (4.76), we obtain the scattering function of a polymer mixture. It is given by the following equation:

$$S_c(\boldsymbol{q}) = \left(\frac{1}{N_A\phi} + \frac{1}{N_B(1-\phi)} - 2\chi + \tilde{v}_c\beta'' q^2\right)^{-1} \ . \tag{4.81}$$

The result allows a reconsideration of the open question about the functional form of the coupling coefficient β''. Insight results from a view on the limiting properties of the scattering function for low concentrations of the polymers A and B, respectively. For the discussion it is advantageous to change to the reciprocal of the scattering function, since this leads to a separation of the contributions of the A's and B's

$$\frac{1}{S_c} = \frac{1}{N_A\phi} + \frac{1}{N_B(1-\phi)} - 2\chi + \tilde{v}_c\beta'' q^2 \ . \tag{4.82}$$

First consider the limit $\phi \to 0$. When A is the minority species, present only in low concentration, our equation gives

$$\frac{1}{S_c} \to \frac{1}{\phi N_A} + \tilde{v}_c\beta'' q^2 \ . \tag{4.83}$$

On the other hand, for this case, the exact form of S_c is known. Since in melts polymer chains are ideal, S_c is given by the Debye structure function (Eqs. (2.60) and (2.61)), multiplied by the volume fraction ϕ in order to account for the dilution

$$S_c = \phi N_A S_D(R_A^2 q^2) \ . \tag{4.84}$$

Using the series expansion Eq. (2.63) we may write

$$\frac{1}{S_c} \approx \frac{1}{N_A\phi}\left(1 + \frac{R_A^2 q^2}{18}\right) \ . \tag{4.85}$$

Equivalently, when choosing polymer B as the diluted species, our equation leads to

$$\frac{1}{S_\mathrm{c}} \to \frac{1}{(1-\phi)N_\mathrm{B}} + \tilde{v}_\mathrm{c}\beta'' q^2 \,, \tag{4.86}$$

whereas the complete expression is

$$\frac{1}{S_\mathrm{c}} = \frac{1}{(1-\phi)N_\mathrm{B} S_\mathrm{D}(R_\mathrm{B}^2 q^2)} \tag{4.87}$$

$$\approx \frac{1}{N_\mathrm{B}(1-\phi)} \left(1 + \frac{R_\mathrm{B}^2 q^2}{18}\right) \,. \tag{4.88}$$

A comparison of Eq. (4.83) with Eq. (4.85) and Eq. (4.86) with Eq. (4.88) gives us an explicit expression for the coupling constant β'': Equations agree for

$$\beta'' = \frac{1}{\tilde{v}_\mathrm{c}} \frac{R_\mathrm{A}^2}{18 N_\mathrm{A}\phi} + \frac{1}{\tilde{v}_\mathrm{c}} \frac{R_\mathrm{B}^2}{18 N_\mathrm{B}(1-\phi)} \,. \tag{4.89}$$

Inserting this expression into Eq. (4.82), we obtain as the final result

$$\frac{1}{S_\mathrm{c}} = \frac{1}{\phi N_\mathrm{A}} \left(1 + \frac{R_\mathrm{A}^2 q^2}{18}\right) + \frac{1}{(1-\phi)N_\mathrm{B}} \left(1 + \frac{R_\mathrm{B}^2 q^2}{18}\right) - 2\chi \,. \tag{4.90}$$

Is this really correct? Considering the simple Ginzburg–Landau functional, Eq. (4.62), which we chose as our starting point, this is a legitimate question and indeed the comparisons with the known limiting behaviors for $\phi \to 0$ and $(1-\phi) \to 0$ point at limitations. Full agreement in these limits is only reached for $R_\mathrm{A}^2 q^2 \ll 1$, $R_\mathrm{B}^2 q^2 \ll 1$.

One might suspect that these limitations can be removed by an obvious extension of Eq. (4.90). It is possible to construct a scattering function that is correct for the known limits without being restricted to low q's. Evidently this is accomplished by the equation

$$\frac{1}{S_\mathrm{c}} = \frac{1}{\phi N_\mathrm{A} S_\mathrm{D}(R_\mathrm{A}^2 q^2)} + \frac{1}{(1-\phi)N_\mathrm{B} S_\mathrm{D}(R_\mathrm{B}^2 q^2)} - 2\chi \,. \tag{4.91}$$

In fact, Eq. (4.91) represents the correct result. It can be obtained with the aid of a theoretical method superior to the Ginzburg–Landau treatment known as the **random phase approximation**. The interested reader finds the derivation in the Appendix, Sect. A.4.1.

The use of Eq. (4.91) enables us to make an evaluation of scattering experiments, in particular

- a determination of the Flory–Huggins parameter χ and the coil sizes $R_\mathrm{A}, R_\mathrm{B}$;
- a determination of the spinodal, based on the temperature dependence of the concentration fluctuations in the homogeneous phase.

We reduce the discussion again to the case of symmetric polymer mixtures with

$$N_{\mathrm{A}} = N_{\mathrm{B}} = N$$

and apply Eq. (4.90), now in the form

$$\begin{aligned}\frac{1}{S_{\mathrm{c}}} &= \frac{1}{N}\frac{1}{\phi(1-\phi)} + \frac{q^2}{18N}\left(\frac{R_{\mathrm{A}}^2}{\phi} + \frac{R_{\mathrm{B}}^2}{1-\phi}\right) - 2\chi \\ &= \frac{1}{N}\frac{1}{\phi(1-\phi)} + \frac{1}{N\phi(1-\phi)}\frac{q^2}{18}R_\phi^2 - 2\chi\,. \end{aligned} \tag{4.92}$$

In the last equation we have introduced a ϕ-dependent average over the coil radii, R_ϕ, defined as

$$R_\phi^2 = (1-\phi)R_{\mathrm{A}}^2 + \phi R_{\mathrm{B}}^2\,. \tag{4.93}$$

Applying Eq. (4.54), we may also write

$$\frac{1}{S_{\mathrm{c}}} = 2(\chi_{\mathrm{sp}} - \chi) + 2\chi_{\mathrm{sp}}\frac{R_\phi^2}{18}q^2\,. \tag{4.94}$$

Equation (4.94) enables us to make a determination of χ and R_ϕ for a (symmetric) polymer mixture. Figure 4.18 presents, as an example, results of small angle X-ray scattering experiments, carried out on mixtures of polystyrene and partially brominated polystyrene ($\mathrm{PBr}_x\mathrm{S}$, with $x = 0.17$). Data are represented by a plot S_{c}^{-1} versus q^2, as suggested by Eq. (4.94). The difference in slopes indicates a change of R_ϕ with the composition, telling us that the coil sizes of polystyrene and the partially brominated polystyrene are different (analysis of the data yielded $R(\mathrm{PS}) = 32\,\text{Å}$, $R(\mathrm{PBr}_x\mathrm{S}) = 39\,\text{Å}$). The bottom part of Fig. 4.18 presents the values derived for χ, together with χ_{sp} according to Eq. (4.54). Results show that χ is not a constant, although the changes are comparatively small. Strictly speaking, the measurement yields Λ (Eq. (4.58)) rather than χ, but the difference seems negligible.

An understanding of the microscopic origin of the observed ϕ-dependence on theoretical grounds is difficult and this is a situation where computer simulations can be quite helpful. In fact, computations for a lattice model have led to qualitatively similar results, as demonstrated by the curves depicted in Fig. 4.19. These curves all exhibit the slight curvature of the experimental curves. A second result of the simulations is particularly noteworthy. Computer simulations can be used for general checks of the assumptions of the Flory–Huggins model, which cannot be accomplished in an easy manner by analytical considerations. In the example, computations were carried out for a simple cubic lattice. In order to reduce the 'equilibration time' in the computer, as given by the number of steps necessary to reach the equilibrium when starting from an arbitrary configuration, 20% of the lattice sites were

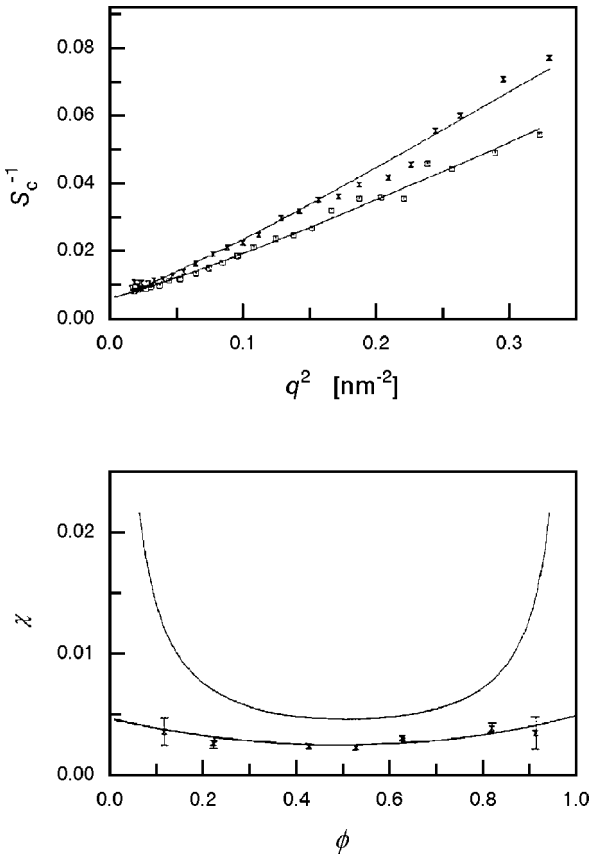

Fig. 4.18. Results of SAXS experiments on mixtures of PS and PBr_xS, both species having equal degrees of polymerization ($N = 430$). Scattering functions for $\phi(\mathrm{PS}) = 0.42$ and 0.62 (*top*) and derived function $\chi(\phi)$ (*bottom*). The *upper curve* in the lower figure represents χ_{sp} [24]

left empty. Calculations were carried out for different values of χ'. We discussed the predictions of the Flory–Huggins model and expect from it, for a dense system, the relation Eq. (4.8)

$$(\Lambda =)\chi = z_{\mathrm{eff}}\chi' \,. \tag{4.95}$$

The simulation yielded consistently lower values, i.e.,

$$\Lambda < z_{\mathrm{eff}}\chi' \,. \tag{4.96}$$

There is first a trivial reason, given by the presence of the vacancies that reduce the interaction energy, but this contributes only a factor of about 0.8. The observed difference is definitely larger and this points at deficiencies

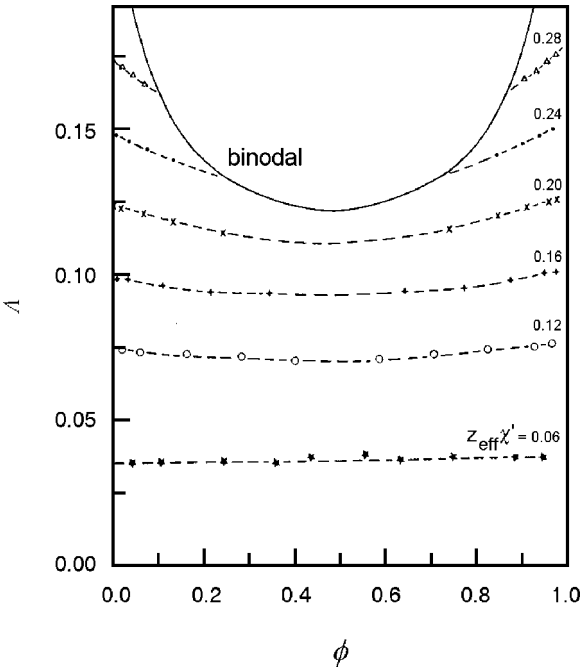

Fig. 4.19. Results obtained in a Monte-Carlo simulation for a lattice model of a polymer mixture ($N_A = N_B = 16$; simple cubic lattice, i.e., $z_{eff} = 4$; 80% of the lattice are occupied by the chains). Calculation of the function $\Lambda(\phi)$ for different values of $z_{eff}\chi'$ ($\phi = \phi_A/(\phi_A + \phi_B)$ is the relative concentration of A-chains). Calculation by Sariban and Binder [25]

of the mean field approximation in the description of this model system. Obviously, the number of AB-contacts is smaller than expected under the assumption of a random distribution of the chains. A closer inspection of the data indicated an enhanced number of intramolecular contacts and also some intermolecular short-range order. Hence, the simulation tells us, as a general kind of warning, that one should be careful in interpreting measured χ-parameters. There can always be perturbing effects. Shortcomings of the Flory–Huggins treatment show up in particular if the molar masses are low. Some effects emerge only for such systems, an important one being the short-range ordering mentioned above. Short-range order effects can only arise if the distances over which the concentration fluctuations are correlated are larger than or similar to the chain size. Conversely, for chains with sufficiently high degrees of polymerization, short-range order effects are ruled out; chains actually average over all local concentration fluctuations and experience the mean value of the contact energies only. In our case, both the experiment and the simulation refer to moderate or even low degrees of polymerization and the qualitative comparison appears justified.

Next, let us return once again to Fig. 4.15, which shows temperature dependent measurements on mixtures of deutero-polystyrene and poly(vinylmethyl-ether). Now, we can recognize the theoretical basis of the chosen representation S^{-1} versus q^2, namely as corresponding to Eq. (4.91). A change in temperature with the resulting change in χ leads to a parallel shift of the curve $S^{-1}(q^2)$. The right part of the figure shows the limiting value $S^{-1}(q \to 0)$ as a function of temperature, directly expressing the T-dependence of χ according to

$$\frac{1}{S_{\mathrm{c}}(q \to 0)\tilde{v}_{\mathrm{c}}} = \frac{2(\chi_{\mathrm{sp}} - \chi)}{\tilde{v}_{\mathrm{c}}} \,. \tag{4.97}$$

For $\chi(T)$ the observed straight line indicates a linear dependence

$$\chi_{\mathrm{sp}} - \chi \propto T^{-1} - T_{\mathrm{sp}}^{-1} \,. \tag{4.98}$$

If we wish to account for both upper and lower miscibility gaps, we may write in linear approximation

$$\chi_{\mathrm{sp}} - \chi \propto \; |T - T_{\mathrm{sp}}| \tag{4.99}$$

and thus expect a temperature dependence

$$S^{-1}(0) \propto \; |T - T_{\mathrm{sp}}| \,. \tag{4.100}$$

The data in Fig. 4.15 were obtained for a mixture with the critical concentration and here the extrapolation to the point where $S_{\mathrm{c}}(0)$ diverges yielded the critical temperature. We can now also see the procedure to be used for a determination of the complete spinodal. One has to carry out temperature-dependent measurements for a series of mixtures, which cover the whole range of compositions. Extrapolations on the basis of Eq. (4.100), i.e., a continuation of the temperature-dependent $S_{\mathrm{c}}^{-1}(0)$ down to zero, yields the spinodal $T_{\mathrm{sp}}(\phi)$, as represented in a (ϕ, T)-phase diagram. Figure 4.20 shows, as an example, a respective set of data that was obtained in another neutron scattering study on mixtures of deuterated polystyrene and poly(vinylmethylether). The linear relation Eq. (4.100) appears verified and the corresponding extrapolations then yield the spinodal depicted in the lower half of the figure.

The concentration fluctuations in a mixture are spatially correlated, with the degree of coupling decreasing with the distance. We may inquire about the **correlation length** of the fluctuations, i.e., the maximum distance over which correlations remain essential. The answer follows from the scattering function. Rewriting Eq. (4.94), we obtain for the small angle range a curve with Lorentzian shape,

$$S_{\mathrm{c}} = \frac{1}{2(\chi_{\mathrm{sp}} - \chi)} \frac{1}{1 + \xi_{\phi}^2 q^2} \,. \tag{4.101}$$

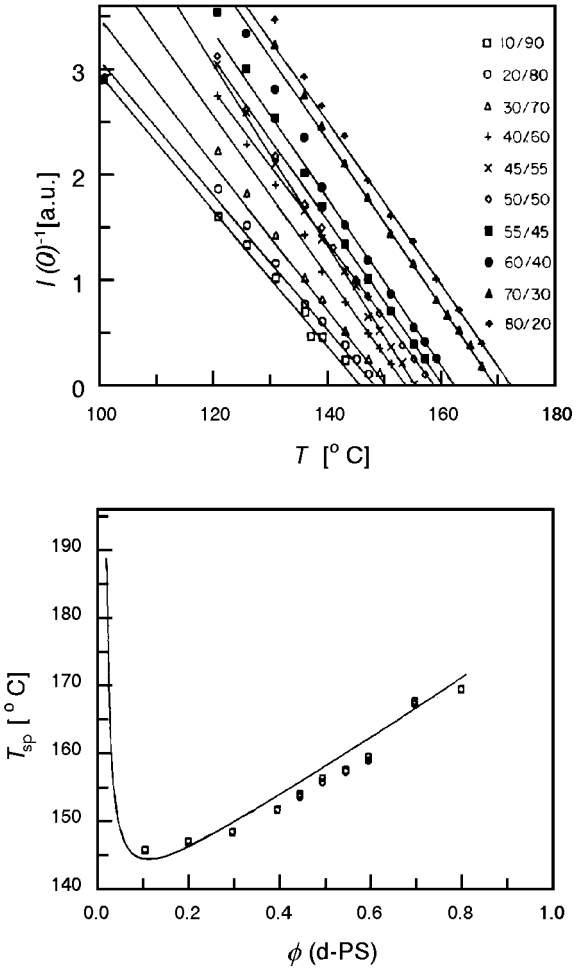

Fig. 4.20. Spinodal of a mixture of d-PS ($M = 5.93 \times 10^5\,\mathrm{g\,mol^{-1}}$) and PVME ($M = 1.1 \times 10^6\,\mathrm{g\,mol^{-1}}$) (*bottom*) as derived from the temperature dependence of neutron scattering intensities in forward direction (*top*). Data from Han et al. [26]

The parameter ξ_ϕ^2 is given by

$$\xi_\phi^2 = \frac{\chi_{\mathrm{sp}} R_\phi^2}{18(\chi_{\mathrm{sp}} - \chi)} \,. \tag{4.102}$$

ξ_ϕ represents the correlation length, as is revealed by a Fourier transformation of S_c. It yields the correlation function for the concentration fluctuations in direct space

$$\langle \delta\phi(0)\delta\phi(\boldsymbol{r})\rangle \propto \int \exp(\mathrm{i}\boldsymbol{q}\boldsymbol{r}) S_\mathrm{c}(\boldsymbol{q})\,\mathrm{d}^3\boldsymbol{q} \tag{4.103}$$

(if an explanation is necessary, look at the derivation of Eq. (A.17) in the Appendix). The evaluation is straightforward and leads to

$$\langle \delta\phi(0)\delta\phi(\boldsymbol{r})\rangle \propto \frac{1}{r}\exp -\frac{r}{\xi_\phi} \; . \tag{4.104}$$

As we can see, ξ_ϕ indeed describes the spatial extension of the correlations.

In all second order phase transitions, the correlation length of the fluctuations of the order parameter diverges at the critical point. We also find this behavior in our system, when making use of Eq. (4.100). For the temperature dependence of ξ_ϕ we obtain the power law

$$\xi_\phi \propto (\chi_{\rm sp} - \chi)^{-1/2} \propto \; |T - T_{\rm sp}|^{-1/2} \; . \tag{4.105}$$

If an experiment is conducted for the critical composition $\phi_{\rm c}$, then one observes the divergence of ξ_ϕ. For concentrations different from $\phi_{\rm c}$, the increase of ξ_ϕ stops when the binodal is reached.

4.3.2 Decomposition Kinetics

After having crossed the spinodal, either through the critical point or somewhere else by a rapid quench that passes quickly through the nucleation and growth range, unmixing sets in by the mechanism known as spinodal decomposition. Measurements like the ones presented in Figs. 4.16 and 4.17 allow detailed investigations. The experiments yield the time-dependent **transient scattering function**, which we denote as $S_{\rm tr}(q,t)$.

Theory has succeeded to derive an **equation of motion** for $S_{\rm tr}(q,t)$, which can be used for an analysis of the kinetics of structure evolution in the early stages of development. It has the following form:

$$\frac{{\rm d}S_{\rm tr}(q,t)}{{\rm d}t} = -\Gamma(q)(S_{\rm tr}(q,t) - S_{\rm c}(q)) \; . \tag{4.106}$$

$S_{\rm c}$ is defined by Eq. (4.91) and $\Gamma(q)$ is a rate constant, determined by

$$\Gamma(q) = 2q^2\lambda(q)S_{\rm c}^{-1}(q) \; . \tag{4.107}$$

λ is a function that relates to the single chain dynamics in the mixture.

A derivation of this equation lies outside our scope, so that we can only consider briefly its background and some implications. First of all, note that Eq. (4.106) has the typical form of a first order relaxation equation, as it is generally used to describe irreversible processes that bring a system from an initial non-equilibrium state back to equilibrium. Therefore, if rather than crossing the spinodal, the temperature jump is carried out within the one phase region, causing a transition of the structure into a new state with higher or lower concentration fluctuations, then the applicability of the equation is unquestionable. Indeed, Eq. (4.106) is meant to cover this 'normal' case as

well. S_c then represents the structure factor associated with the new equilibrium state. The different factors included in the equation for the relaxation rate Γ are all conceivable. A quadratic term in q always shows up for particle flows based on diffusive motions and these have to take place if a concentration wave is to alter its amplitude. Its background is of a twofold nature and easily seen. Firstly, according to Fick's law, flow velocities are proportional to concentration gradients and thus proportional to q. Secondly, with increasing wavelength, particles have to go over correspondingly larger distances and this produces a second factor q. Both effects together give the characteristic q^2. The origin of the factor S_c^{-1} is revealed by a look at Eqs. (4.74) and (4.82). Equation (4.74) is formally equivalent to the energy (u)-displacement (x) relation of a harmonic oscillator

$$u = \frac{1}{2} a x^2 \ . \tag{4.108}$$

We therefore may also address the factor in Eq. (4.74), which corresponds to a as a 'stiffness coefficient', now related to the formation of a concentration wave. Interestingly enough, exactly this stiffness coefficient shows up again in Eq. (4.82) for S_c^{-1}, apart from a trivial factor $\tilde{R}T/\tilde{v}_c$. As S_c^{-1} is determined by this factor only, it can replace the stiffness coefficient in equations. Clearly, the latter affects the relaxation rate and therefore has to be part of any equation for Γ. Since our system shows close similarities to an overdamped harmonic oscillator, both having the same equation of motion, we can also understand the linear dependence of Γ on S_c^{-1}. Hence in conclusion, for temperature jumps within the one phase region, Eq. (4.106) looks perfectly reasonable. It may appear less obvious that its validity is maintained if temperature jumps transfer the system into the two-phase region so that spinodal decomposition sets in. One could argue that, in view of the continuous character of critical phase transitions, one could expect the same kinetic equations to hold on both sides of the phase boundary, but a direct proof is certainly necessary and is indeed provided by the theoretical treatments.

A change occurs in the meaning of S_c. For temperatures in the two-phase region, S_c can no longer be identified with an equilibrium structure function. Nevertheless, its definition by Eq. (4.91) is maintained. This implies that S_c shows negative values at low q's, being positive only for high q's. Here we are dealing with a **virtual structure function**, which is not a measurable quantity but defined by an extrapolation procedure. In order to obtain S_c, one has to determine the temperature dependence of χ in the homogeneous phase, introduce it into Eq. (4.91) and use this equation also for temperatures in the two-phase region.

The specific character of the spinodal decomposition can now be understood as being a consequence of the peculiar q-dependence of the rate constant Γ. Figure 4.21 presents results of a calculation applying Eq. (4.107). For q's below a critical value q_c, S_c^{-1} and therefore $\Gamma(q)$ take on negative values. A negative value of Γ indicates an amplitude growth, instead of the usual

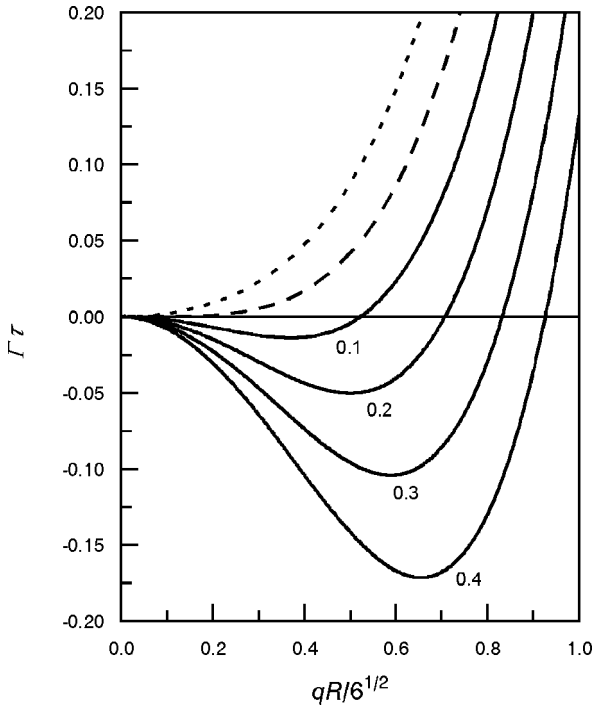

Fig. 4.21. Rate constants Γ determining the time-dependent changes of the structure function of a symmetric polymer mixture ($R_A = R_B = R$) after a temperature jump from the homogeneous phase ($\chi < \chi_{sp}$) into the two-phase region ($\chi > \chi_{sp}$) (*continuous lines*). Curves correspond to different distances from the spinodal, $(\chi - \chi_{sp})/\chi_{sp} = 0.1 - 0.4$ and were obtained applying Eqs. (4.107), (4.91) ($\tau = NR^2\phi(1-\phi)/6\lambda(0)$). The *dashed line* gives the rate constants at the spinodal, the *dotted line* those associated with a temperature jump within the one phase region to $\chi/\chi_{sp} = 0.9$

decay. The main feature in the curve is the maximum in the growth rate, $-\Gamma$, at a certain value q_{max} somewhere in the range

$$0 < q_{max} < q_c \ .$$

Structure evolution is controlled by the concentration waves with wavevectors around q_{max}. These constitute the dominant modes of structure formation and determine the length scale of the pattern during the early stages of development. Figure 4.21 also indicates the temperature dependence of q_{max} and the largest associated growth rate. We see that the approach of the spinodal in the two-phase region is accompanied by a decrease of q_{max}. Straightforward analysis shows that the decrease obeys the power law

$$q_{max} \propto (\chi - \chi_{sp})^{1/2} \propto |T_{sp} - T|^{1/2} \ . \tag{4.109}$$

Simultaneously, a slowing down of the growth rate occurs according to

$$-\Gamma(q_{\max}) \propto -q_{\max}^2 S_{\rm c}^{-1}(q_{\max}) \; . \tag{4.110}$$

Employing Eq. (4.94) we obtain

$$-\Gamma(q_{\max}) \propto -q_{\max}^2 \left((\chi_{\rm sp} - \chi) + \chi_{\rm sp} \frac{R_\phi^2}{18} q_{\max}^2 \right) \propto |T_{\rm sp} - T|^2 \; . \tag{4.111}$$

This **critical slowing down** also shows up on the other side of the phase boundary, when for a critical mixture the critical temperature is approached from the one phase region. The kinetic parameter of interest, to be used on both sides, is the **collective diffusion coefficient**, $D_{\rm coll}$, defined as

$$D_{\rm coll} = \lim(q \to 0) \frac{\Gamma(q)}{2q^2} \; , \tag{4.112}$$

and it is given by

$$D_{\rm coll} = \lambda(0) S_{\rm c}(0)^{-1} \; . \tag{4.113}$$

The attribute 'collective' is used in order to distinguish this parameter from the **self-diffusion coefficient** of the individual chains, which relates to the single chain dynamics as expressed by λ only, and therefore shows no critical slowing down. We see that $D_{\rm coll}$ takes on positive and negative values, crossing zero at the spinodal

$$D_{\rm coll} \propto \chi_{\rm sp} - \chi \propto \pm |T - T_{\rm sp}| \; . \tag{4.114}$$

Equation (4.106) can be solved exactly and the solution is

$$S_{\rm tr}(q,t) = S_{\rm c}(q) + (S_{\rm tr}(q,0) - S_{\rm c}(q)) \exp[-\Gamma(q)t] \; . \tag{4.115}$$

Figure 4.22 presents the results of model calculations performed on the basis of this equation. We find that a spinodal decomposition leads to an intensity increase for all q's, with a maximum at a certain $q_{\max}$. Growing in intensity, the peak stays at a fixed position. In the long time limit we observe an exponential law

$$S_{\rm tr}(q_{\max}) \propto \exp(-\Gamma t) \; . \tag{4.116}$$

As we can see, the model calculations reproduce the main features of the experimental observations during the initial stages of spinodal decompositions. In fact, the equations can be applied for a representation of experimental data and we refer here once again to the measurement presented in Fig. 4.16. Figure 4.23 shows a plot on the left-hand side according to

$$\ln \frac{S_{\rm tr}(q,t) - S_{\rm c}(q)}{S_{\rm tr}(q,0) - S_{\rm c}(q)} = \ln \frac{\Delta S(q,t)}{\Delta S(q,0)} = -\Gamma(q) t \; . \tag{4.117}$$

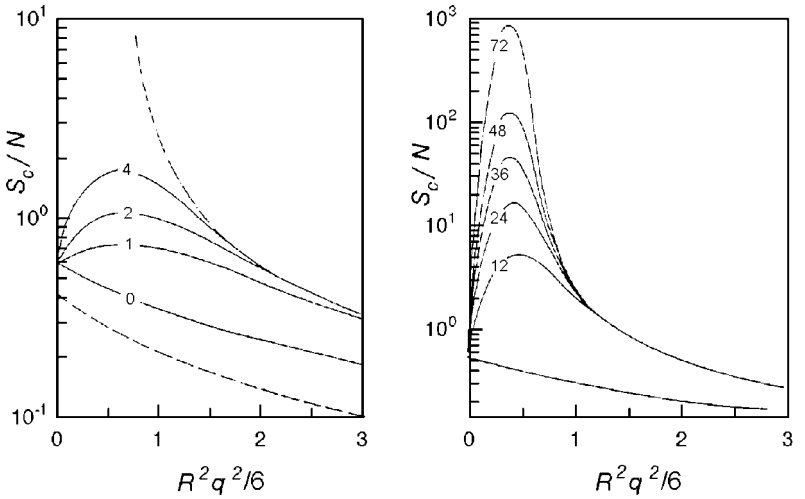

Fig. 4.22. Spinodal decomposition initiated by a jump from the one phase region ($N\chi = 1$) to the two-phase region ($N\chi = 2.5$). Model calculation for a symmetric polymer blend ($N_A = N_B = N, R_A = R_B = R$) on the basis of Eqs. (4.115), (4.107), (4.91). The *numbers* represent units of time [27]

The virtual structure function $S_c(q)$ has been constructed by a linear extrapolation of the equilibrium values in the homogeneous region shown in Fig. 4.15; the change from positive to negative values occurs for $q_c = 2.9 \times 10^{-2}\,\mathrm{nm}^{-1}$. For all q's we find exponential time dependencies in agreement with Eq. (4.115). The derived rate constants Γ are given by the lowest curve (134.1 °C) on the right-hand side. One has negative values for $q < q_c$ and in this range a maximum in the growth rate. In addition, the right-hand figure includes the results of two other experiments, one conducted at $T = 133\,^\circ\mathrm{C}$, even closer to T_c, and the other at $T = 131.85\,^\circ\mathrm{C}$, which is in the one phase region. One observes a shift of q_{max} towards zero for $T \to T_c$ and on both sides of T_c a critical slowing down for $D_{coll} \propto \mathrm{d}^2\Gamma/\mathrm{d}q^2(q = 0)$, which is in full agreement with the theoretical predictions.

Late Stage Kinetics

The described initial stages of spinodal decomposition constitute the entrance process, thereby setting the basic structure characteristics and the primary length and time scales. They represent a first part only, coming to an end when the concentration waves produce, in summary, variations $\delta\phi$, which already approach the concentrations of the two equilibrium phases. Then the exponential increase of the amplitudes cannot continue further and the kinetics must change. A first natural effect is a retardation of the growth rate, and a second is a shift of q_{max} towards lower values. An example for this generally observed behavior was presented in Fig. 4.17 with the light scattering curves

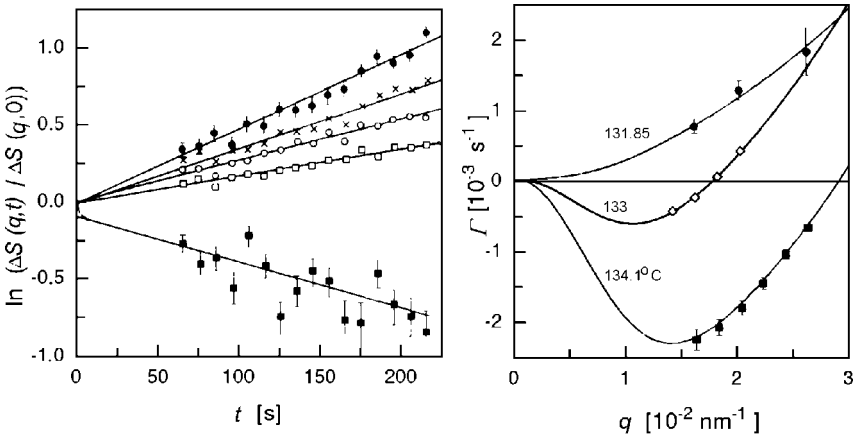

Fig. 4.23. Same system as in Figs. 4.15 and 4.16 [22]. Plot demonstrating an exponential time dependence of the transient scattering intensities at $T = 134.1\,^{\circ}\mathrm{C}$ for different q's (1.79×10^{-2}; 2.2×10^{-2}; 2.4×10^{-2}; 2.6×10^{-2}; $3.62 \times 10^{-2}\,\mathrm{nm}^{-1}$) (*left*). Derived rate constants $\Gamma(q)$ for growth ($\Gamma < 0$) or decay ($\Gamma > 0$), together with the results of equivalent experiments for $T = 133\,^{\circ}\mathrm{C}$ ($> T_c = 131.9\,^{\circ}\mathrm{C}$) and $T = 131.85\,^{\circ}\mathrm{C}$ ($< T_c$) (*right*)

obtained for a polystyrene/poly(vinylmethylether) mixture. Theory has dealt with these first changes by a generalization of the linear equations valid for the initial stages and accounting for the saturation effects introduced by the bounds. Treatments are rather involved and we cannot present them here. Interestingly enough, after this second period, there follows a third part where behavior again becomes simpler. This is the regime of the **late stage kinetics** and we will briefly describe some major observations in this section.

The micrograph on the right-hand side of Fig. 4.10 was obtained during this late stage of structure evolution and represents an instructive example. The interconnected domains are set up by the two equilibrium phases. The interfaces are well-established and it can be assumed that their microscopic structure, as described by the concentration profile of the transition zone, has also reached the equilibrium form. Further observations for the same system, a mixture of polystyrene and partially brominated polystyrene, are included in Fig. 4.24. The three micrographs were obtained at somewhat earlier times. Although the observed structures are finer and therefore less well-resolved, it seems clear that they are identical in their general character. What we see here is a coarsening process and, importantly, the observations suggest that all these transient structures which are passed through during the late stages of unmixing are similar to each other and differ only in length scale. It is possible to checks for the suspected similarity by light scattering experiments. Figure 4.25 depicts, as an example, scattering curves obtained for a mixture of polybutadiene (PB) and polyisoprene (PI).

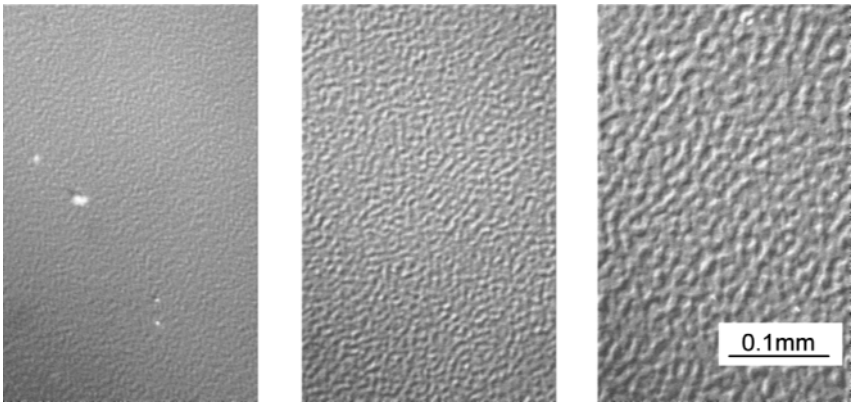

Fig. 4.24. Structure development during the late stages of spinodal decomposition observed for a PS/PBr$_x$S-(1:1) mixture. Micrographs were obtained during annealing at 200 °C ($< T_c = 220$ °C) for 1 min (*left*), 3 min (*center*) and 10 min (*right*) [21]

Here a spinodal decomposition can be initiated by a temperature jump into an upper miscibility gap. Similarity implies that in a representation with reduced variables, plotting $\log(I/I_{\max})$ versus $\log(q/q_{\max})$, curves measured at different times must become identical. As we can see, this is indeed true. We notice in addition that even the structures observed at different temperatures are similar to each other. We thus have a most simple situation that allows us to describe the kinetics of unmixing by the time dependence of just one parameter. Possible choices are either $q_{\max}^{-1}$, representing a typical length in the structure, or the interfacial area per unit volume, denoted by O_{12}. In fact, both quantities are related. Two-phase systems in general have two primary structure parameters, namely the volume fraction of one phase, ϕ, and O_{12}. As explained in Sect. A.4.2 in the Appendix, from ϕ and O_{12} one can derive a characteristic length of the structure, l_c, as

$$l_c = \frac{2\phi(1-\phi)}{O_{12}} \tag{4.118}$$

(see Eq. (A.161)). l_c and $q_{\max}^{-1}$ have equal orders of magnitude and are proportional to each other

$$l_c = \text{const } q_{\max}^{-1} , \tag{4.119}$$

the proportionality constant depending on the structure type. Clearly, when the formation of the equilibrium phases is completed for the first time, ϕ is fixed and does not change any more. Hence from this point on, throughout the late stages of unmixing, one must find a strict inverse proportionality between l_c or $q_{\max}^{-1}$ and O_{12}. O_{12} can be directly derived from the scattering curve us-

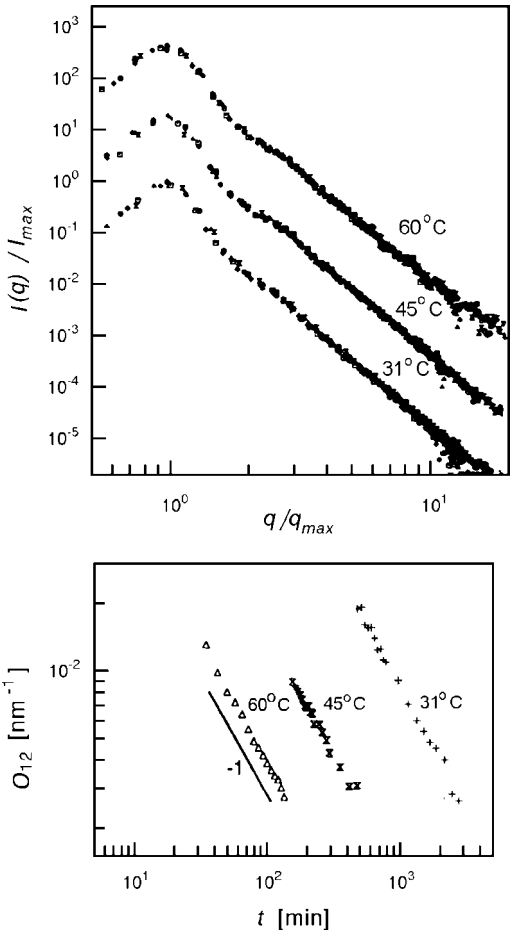

Fig. 4.25. Light scattering curves obtained for a PB ($M = 5.8 \times 10^5\,\mathrm{g\,mol^{-1}}$)/PI ($M = 1 \times 10^5\,\mathrm{g\,mol^{-1}}$)-(1:1) mixture during the late stage of spinodal decomposition at the indicated temperatures (*top*; curves for 45 °C and 60 °C are shifted by constant amounts in vertical direction). Each curve contains measurements for different times and these superpose exactly. Time dependence of the interfacial area per unit volume, O_{12}, in agreement with a power law $O_{12} \propto t^{-1}$, as indicated by the straight line with slope -1 (*bottom*). Data from Takenaka and Hashimoto [28]

ing **Porod's law** (Eq. (A.159)), which states that the scattering function of a two-phase system generally shows an asymptotic behavior according to the power law

$$S(q \to \infty) \propto \frac{O_{12}}{q^4}\ . \tag{4.120}$$

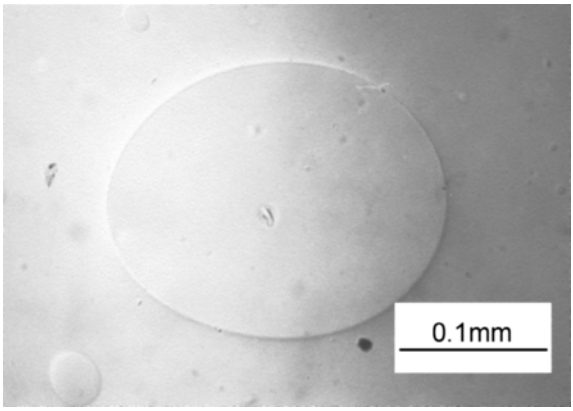

Fig. 4.26. Macroscopic domains in a two-phase PS/PBr$_x$S-(1:1) mixture, formed after 2 h of annealing [21]

The curves in Fig. 4.25 are in agreement with this law, which can therefore be employed for a determination of O_{12}. The time dependence of O_{12} is given in the lower half of Fig. 4.25. Results indicate a decrease of O_{12} inverse to t,

$$O_{12} \propto t^{-1} \,. \tag{4.121}$$

Here, we cannot discuss the theories developed for the late stage kinetics, but the physical background must be mentioned, since it is basically different from the initial stages discussed above. Whereas the kinetics in the initial stages is based on diffusive processes only, the late stages are controlled by convective flow. The driving force originates from the excess free energy of the interfaces. The natural tendency is a reduction of O_{12} and this is achieved by a merging of smaller domains into larger ones.

The latter mechanism remains effective up to the end; however, the structure characteristics must finally change as the similarity property cannot be maintained. The very end is a macroscopic phase separation, as shown, for example, in Fig. 4.26 and clearly, the final structure is always of the same type independent of whether phase separation has started by spinodal decomposition or by nucleation and growth.

4.4 Block Copolymer Phases

If two different polymeric species are coupled together by chemical links, one obtains block copolymers. These materials possess peculiar properties and we will consider them in this section.

In the discussion of the behavior of binary polymer mixtures, we learned that, in the majority of cases, they separate into two phases. As the linkages in block copolymers inhibit such a macroscopic phase separation, one may

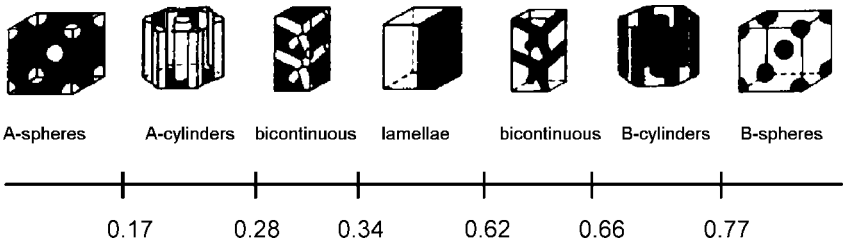

Fig. 4.27. Different classes of microphase separated structures in block copolymers, as exemplified by PS-*block*-PI. The *numbers* give the phase boundaries in terms of the volume fraction of the PS blocks. Figure taken from a review article by Bates and Frederickson [29]

wonder how these systems react under comparable conditions. Figure 4.27 gives the answer with a drawing: The A's and B's still segregate but the domains have only mesoscopic dimensions corresponding to the sizes of the single blocks. In addition, as all domains have a uniform size, they can be arranged in regular manner. As a result ordered mesoscopic lattices emerge. In the figure it is also indicated that this **microphase separation** leads to different classes of structures in dependence on the ratio between the degrees of polymerization of the A's and B's. For $N_A \ll N_B$ spherical inclusions of A in a B-matrix are formed and they set up a body-centered cubic lattice. For larger values N_A, but still $N_A < N_B$, the A-domains have a cylindrical shape and are arranged in a hexagonal lattice. Layered lattices form under essentially symmetrical conditions, i.e., $N_A \approx N_B$. Then, for $N_A > N_B$, the phases are inverted and the A-blocks now constitute the matrix.

In addition to these lattices composed of spheres, cylinders and layers, periodic structures occur under special conditions where both phases are continuous and interpenetrate each other. These bicontinuous **gyroid** structures exist only in a narrow range of values N_A/N_B, between the regimes of the cylindrical and lamellar structures and, as it appears, only when the repulsion forces between the A's and the B's are not too strong. To be sure, the figure depicts the structures observed for polystyrene-*block*-polyisoprene, but these are quite typical. Spherical, cylindrical and layer-like domains are generally observed in all block copolymers. Less is known about how general the bicontinuous special types like the gyroid lattices are.

The majority of synthesized compounds are **di-block copolymers** composed of one A-chain and one B-chain; however, tri-blocks and multiblocks, comprising an arbitrary number of A-chains and B-chains, can be prepared as well. One can also proceed one step further and build up multiblocks that incorporate more than two species, thus again increasing the variability. The question may arise as to whether all these modifications result in novel structures. In fact, this is not the case. The findings give the impression that at least all block copolymers composed of two species exhibit qualitatively sim-

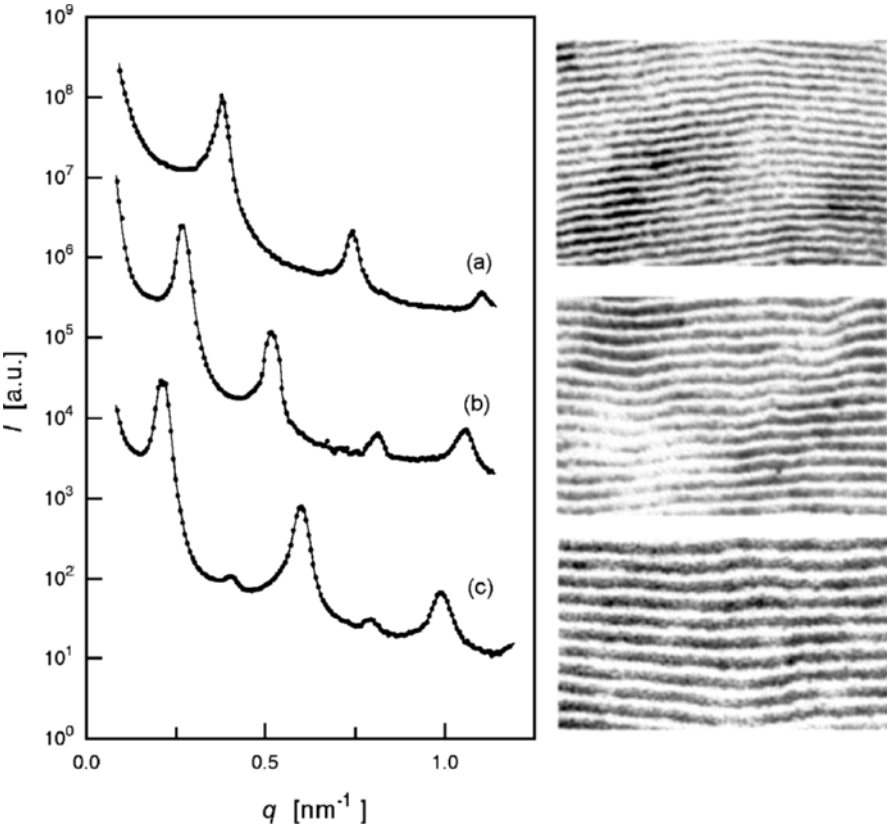

Fig. 4.28. SAXS curves measured for a series of PS-*block*-PI with different molar masses in the microphase separated state: (a) $M = 2.1 \times 10^4\,\mathrm{g\,mol^{-1}}$, $\phi(\mathrm{PS}) = 0.53$; (b) $M = 3.1 \times 10^4\,\mathrm{g\,mol^{-1}}$, $\phi(\mathrm{PS}) = 0.40$; (c) $M = 4.9 \times 10^4\,\mathrm{g\,mol^{-1}}$, $\phi(\mathrm{PS}) = 0.45$ (*left*). Transmission electron micrographs obtained using ultra-thin sections of specimen stained with OsO_4 (*right*). Structures belong to the layer regime. Data from Hashimoto et al. [30]

ilar phase behaviors. Changes then occur for ternary systems. For the latter, the observed structures still possess periodic orders, but the lattices are more complex. Here, we shall only be concerned with the simplest systems, the di-block copolymers.

Suitable methods for an analysis of block copolymer structures are electron microscopy and small angle X-ray scattering (SAXS) experiments. Figure 4.28 gives an example and on the left-hand side presents scattering curves obtained for a series of polystyrene-*block*-polyisoprenes where both blocks had similar molar mass. Structures belong to the layer regime and one correspondingly observes series of equidistant Bragg reflections. The right-hand side depicts micrographs obtained for the same samples in an electron microscope using

ultra-thin sections of specimens where the polyisoprene blocks were stained with OsO_4. The layered structure is clearly visible and one notices an increase of the layer thicknesses with the molar masses of the blocks.

In binary polymer mixtures, under favorable conditions one finds homogeneous phases. They either arise if the forces between unlike monomers are attractive or, generally, if the molar masses are sufficiently low. Block copolymers behave similarly and can also have a homogeneous phase. It actually has a larger stability range than the corresponding binary mixture. Recall that for a symmetric mixture ($N_A = N_B$) the two-phase region begins at (Eq. (4.35))

$$(\chi N_A)_c = 2 \, .$$

If a symmetric di-block copolymer is formed from the same A- and B-chains, the transition between the homogeneous phase and the microphase separated state takes place at a higher χ, namely for

$$(\chi N_A)_c \approx 5 \, . \tag{4.122}$$

The complete phase diagram of a block copolymer is displayed in Fig. 4.29 in a schematic representation. Variables are the volume fraction of the A-blocks

$$\phi_A = \frac{N_A}{N_A + N_B} \tag{4.123}$$

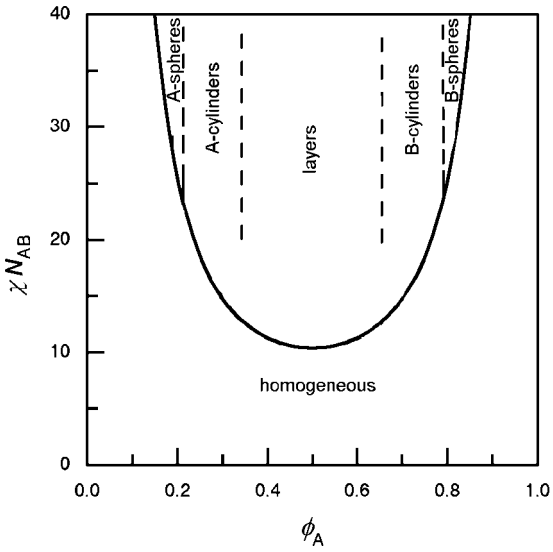

Fig. 4.29. Phase diagram of a di-block copolymer in a schematic representation. The curve describes the points of transition between the homogeneous phase and the microphase separated states. The ordered states are split into different classes as indicated by the *dashed boundary lines*. They are only shown here for the region of higher values of χN_{AB} away from the phase transition line

and the product χN_{AB}, where N_{AB} describes the total degree of polymerization

$$N_{\mathrm{AB}} = N_{\mathrm{A}} + N_{\mathrm{B}} \; .$$

The transition line separating the homogeneous phase from the various microphase separated structures has an appearance similar to the binodal of a polymer mixture. There is, however, a basic difference: In the block copolymer case, we are dealing with a one component system rather than a binary mixture. The line therefore relates to a phase transition rather than to a miscibility gap. It should also be noted that, in contrast to the binodal of a mixture, the transition line tells us nothing about the internal composition of the microphases. In principle, these could be mixed states; however, with the exception of situations near the transition line, compositions are mostly close to pure A- or B-states. The schematic drawing indicates only the structures arising under the conditions of a **strong segregation**, $\chi N_{\mathrm{AB}} \gg 10$, where solely lattices of spheres, cylinders and layers are found. The situation for a **weak segregation** with χN_{AB} just above the critical value is more complicated. Here, also the bicontinuous structures are found and subtle features decide about their stability relative to the three major forms.

4.4.1 Layered Structures

Each of the ordered structures represents under the respective conditions the state with the lowest Gibbs free energy. Calculations of the Gibbs free energies and comparisons between the various lattices and the homogeneous phase can therefore provide an understanding of the phase diagram. In addition, they make it possible to determine the structure parameters.

Theoretical analyses were carried out by Meier and Helfand. A full presentation lies outside our possibilities but in order to gain at least an impression of the approaches, we will pick out the layered structures as an example and discuss the equilibrium conditions. The main result will be a power law that formulates the dependence of the layer thicknesses on the degree of polymerization of the blocks.

If we think about the structural changes that accompany a transition from the homogeneous phase to an ordered layer structure, we find three contributions to the change in the Gibbs free energy

$$\Delta g_{\mathrm{p}} = \Delta h_{\mathrm{p}} - T\Delta s_{\mathrm{p,if}} - T\Delta s_{\mathrm{p,conf}} \; . \tag{4.124}$$

There is a change in enthalpy, a change in entropy following from the arrangement of the junction points along the interfaces and another change in entropy resulting from altered chain conformations. We write the equation in terms of quantities referring to one di-block polymer.

The driving force for the transitions comes from the enthalpic part. In the usual case of unfavorable AB-interactions, i.e., $\chi > 0$, there is a gain

in enthalpy on unmixing. We assume a maximum gain, achieved when we have a random distribution of the monomers in the homogeneous phase and a perfect segregation in the lamellar phase. Then the enthalpy change per polymer, Δh_p, is given by

$$\Delta h_\mathrm{p} = -kT\chi N_\mathrm{AB}\phi_\mathrm{A}(1-\phi_\mathrm{A}) + \Delta h_\mathrm{p,if} \; . \tag{4.125}$$

The first term follows directly from Eq. (4.24). The second term, $\Delta h_\mathrm{p,if}$, accounts for an excess enthalpy that is contributed by the interfaces. To see the background, bear in mind that interfaces always possess a finite thickness, typically in the order of one to several nm. Within this transition layer the A's and B's remain mixed, which leads to an increase in enthalpy proportional to χ and to the number of structure units in the transition layer. Let the thickness of the transition layer be d_t and the interface area per polymer o_p, then we may write

$$\Delta h_\mathrm{p,if} \simeq kT\chi\frac{o_\mathrm{p}d_\mathrm{t}}{v_\mathrm{c}} \; . \tag{4.126}$$

v_c again is the volume of the structure unit, commonly chosen for both the A- and B-chains.

The two entropic parts both work in the opposite direction. There is first the loss in entropy, which results from the confinement of the junction points, being localized in the transition layer. For a layered phase with layer thicknesses d_A and d_B, and therefore a period

$$d_\mathrm{AB} = d_\mathrm{A} + d_\mathrm{B} \; , \tag{4.127}$$

$\Delta s_\mathrm{p,if}$ may be estimated using a standard equation of statistical thermodynamics

$$\Delta s_\mathrm{p,if} \simeq k\ln\frac{d_\mathrm{t}}{d_\mathrm{A}+d_\mathrm{B}} \; . \tag{4.128}$$

The second entropic contribution, $\Delta s_\mathrm{p,conf}$, accounts for a decrease in entropy, which follows from a change in the chain conformations. The Gaussian conformational distribution found in the homogeneous phase cannot be maintained in the microphase separated state. Formation of a layer structure leads, for steric reasons, necessarily to a chain stretching, which in turn results in a loss in entropy. For a qualitative description we employ the previous Eq. (2.93),

$$\Delta s_\mathrm{p,conf} \simeq -k\left(\frac{R}{R_0}\right)^2 \; , \tag{4.129}$$

where R and R_0 are now the end-to-end distances of the block copolymer in the layered and the homogeneous phase, respectively. Assuming that chain sizes and layer spacings are linearly related, by

$$R = \beta d_\mathrm{AB} \; , \tag{4.130}$$

the equation converts into

$$\Delta s_{\mathrm{p,conf}} \simeq -k\beta^2 \left(\frac{d_{\mathrm{AB}}}{R_0}\right)^2 . \tag{4.131}$$

We can now search for the equilibrium. First note that o_{p} and d_{AB} are related by the obvious equation

$$o_{\mathrm{p}} d_{\mathrm{AB}} = N_{\mathrm{AB}} v_{\mathrm{c}} . \tag{4.132}$$

We therefore have only one independent variable, for example o_{p}. Using all the above expressions, we obtain for the change in the Gibbs free enthalpy

$$\frac{1}{kT}\Delta g_{\mathrm{p}} = -\chi N_{\mathrm{AB}} \phi_{\mathrm{A}} (1-\phi_{\mathrm{A}}) + \chi o_{\mathrm{p}} d_{\mathrm{t}} v_{\mathrm{c}}^{-1} + \ln \frac{d_{\mathrm{t}}}{d_{\mathrm{AB}}} + \beta^2 \left(\frac{d_{\mathrm{AB}}}{R_0}\right)^2 . \tag{4.133}$$

If we neglect the slowly varying logarithmic term, we obtain for the derivative

$$\frac{1}{kT}\frac{\mathrm{d}\Delta g_{\mathrm{p}}}{\mathrm{d}o_{\mathrm{p}}} = \chi \frac{d_{\mathrm{t}}}{v_{\mathrm{c}}} - 2\beta^2 \frac{N_{\mathrm{AB}}^2 v_{\mathrm{c}}^2}{R_0^2} \frac{1}{o_{\mathrm{p}}^3} . \tag{4.134}$$

The equilibrium value of o_{p} follows as

$$o_{\mathrm{p}}^3 \propto 2 \frac{v_{\mathrm{c}}^3}{R_0^2 d_{\mathrm{t}} \chi} N_{\mathrm{AB}}^2 . \tag{4.135}$$

With

$$R_0^2 \propto v_{\mathrm{c}}^{2/3} N_{\mathrm{AB}} \tag{4.136}$$

we find

$$o_{\mathrm{p}}^3 \propto \frac{v_{\mathrm{c}}^{7/3}}{d_{\mathrm{t}} \chi} N_{\mathrm{AB}} . \tag{4.137}$$

Replacement of o_{p} by d_{AB} gives us the searched-for result

$$d_{\mathrm{AB}}^3 = \frac{N_{\mathrm{AB}}^3 v_{\mathrm{c}}^3}{o_{\mathrm{p}}^3} \propto \chi d_{\mathrm{t}} v_{\mathrm{c}}^{2/3} N_{\mathrm{AB}}^2 . \tag{4.138}$$

How does this result compare with experiments? Figure 4.30 depicts the data obtained for the samples of Fig. 4.28. Indeed, the agreement is perfect. The slope of the line in the double logarithmic plot exactly equals the predicted exponent 2/3.

4.4.2 Pretransitional Phenomena

A characteristic property of polymer mixtures in the homogeneous phase is the increase of the concentration fluctuations associated with an approaching of the point of unmixing. A similar behavior is found for the homogeneous phase of block copolymers and a first example is given in Fig. 4.31. The figure

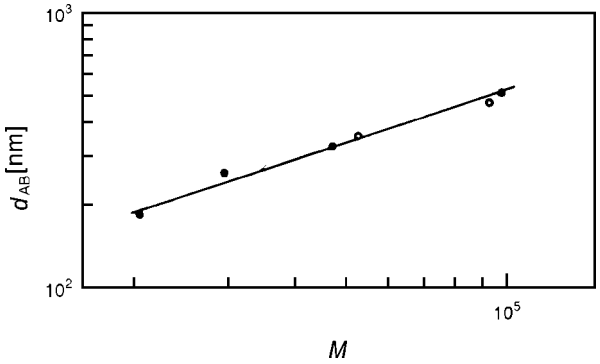

Fig. 4.30. Set of samples of Fig. 4.28. Molecular weight dependence of the layer spacing d_{AB}

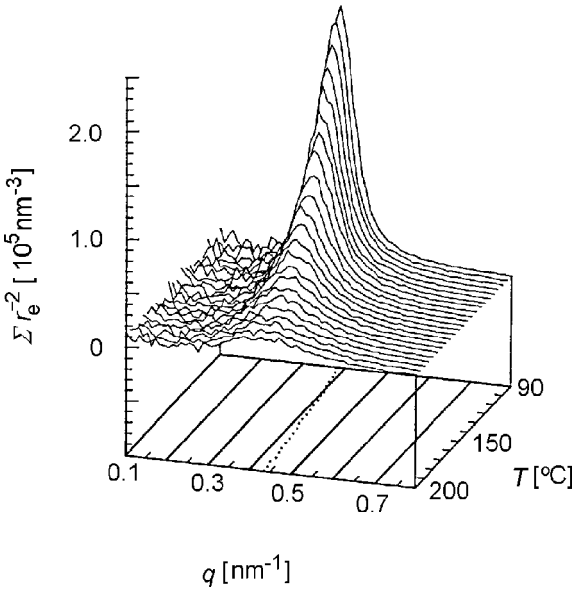

Fig. 4.31. SAXS curves measured for a polystyrene-*block*-polyisoprene ($M = 1.64 \times 10^4\,\mathrm{g\,mol^{-1}}$, $\phi(\mathrm{PS}) = 0.22$) in the homogeneous phase. The *dotted line* on the base indicates the temperature dependence of the peak position [31]

shows scattering functions measured for a PS-*block*-PI under variation of the temperature. The temperature of the transition to the microphase separated state is located around 85 °C, just outside the temperature range of the plot. The curves exhibit a peak, with an intensity that strongly increases when the temperature moves towards the transition point.

The feature in common with the polymer mixtures is the intensity increase; however, we can also see a characteristic difference: The maximum of

the scattering intensity and the largest increase are now found for a finite scattering vector $q_{\max}$, rather than at $q = 0$. As scattering curves display the squared amplitudes of wave-like concentration fluctuations, the observation tells us that concentration fluctuations with wavevectors in the range $|\boldsymbol{k}| \approx q_{\max}$ are always large compared to all the others and show a particularly strong increase on approaching the phase transition. What do these observations mean? Clearly, they remind us of the pretransitional phenomena observed for second order phase transitions. There, the approach of the transition point is always associated with an unusual increase of certain fluctuations. Hence as it appears, one also finds properties in the homogeneous phase that have much in common with the behavior of critical systems, not only for polymer mixtures, but also for block copolymers.

The general shape of the scattering curve, showing a maximum at some $q_{\max}$ and going to zero for $q \to 0$ is conceivable. As explained in Sect. A.3.2 of the Appendix, the forward scattering, $S(q \to 0)$, always relates to the fluctuation of the number of particles in a fixed macroscopic volume. In our case, this refers to both the A's and the B's. The strict coupling between A- and B-chains in the block copolymers completely suppresses number fluctuations on length scales that are large compared to the size of the block copolymer. The limiting behavior of the scattering function, $S(q \to 0) \to 0$, reflects just this fact. On the other hand, for large q's, scattering of a block copolymer and of the corresponding polymer mixture composed of the decoupled blocks, must be identical because here only the internal correlations within the A- and B-chains are of importance. As a consequence, asymptotically the scattering law of ideal chains, $S(q) \propto 1/q^2$, shows up again. Hence, one expects an increase in the scattering intensity coming down from large q's and when emanating from $q = 0$ as well. Both increases together produce a peak, located at a certain finite $q_{\max}$.

The increase of the intensity with decreasing temperature reflects a growing tendency for associations of the junction points accompanied by some short-ranged segregation. As long as this tendency is not too strong, this could possibly occur without affecting the chain conformations, i.e., chains could still maintain Gaussian properties. If one adopts this view, then the scattering function can be calculated explicitly. Leibler and others derived the following expression for the scattering function per structure unit S_{c}:

$$\frac{1}{S_{\mathrm{c}}(q)} = \frac{1}{S_{\mathrm{c}}^{0}(q)} - 2\chi \tag{4.139}$$

with $S_{\mathrm{c}}^{0}(q)$, the scattering function in the athermal case, given by

$$\begin{aligned} S_{\mathrm{c}}^{0}(q) N_{\mathrm{AB}} S_{\mathrm{D}}\left(R_0^2 q^2\right) = {} & \phi(1-\phi) N_{\mathrm{A}} N_{\mathrm{B}} S_{\mathrm{D}}\left(R_{\mathrm{A}}^2 q^2\right) S_{\mathrm{D}}\left(R_{\mathrm{B}}^2 q^2\right) \\ & -\frac{1}{4}\left[N_{\mathrm{AB}} S_{\mathrm{D}}\left(R_0^2 q^2\right) - \phi N_{\mathrm{A}} S_{\mathrm{D}}\left(R_{\mathrm{A}}^2 q^2\right)\right. \\ & \left. -(1-\phi) N_{\mathrm{B}} S_{\mathrm{D}}\left(R_{\mathrm{B}}^2 q^2\right)\right]^2 . \end{aligned} \tag{4.140}$$

R_0^2 denotes the mean squared end-to-end distance of the block copolymer, given by

$$R_0^2 = R_\mathrm{A}^2 + R_\mathrm{B}^2 \; . \tag{4.141}$$

With regard to the effect of χ, Eq. (4.139) is equivalent to Eq. (4.91). Indeed, the physical background of both equations is similar and they are obtained in an equal manner by an application of the random phase approximation (RPA). The interested reader can find the derivation in Sect. A.4.1 in the Appendix.

Importantly, Eq. (4.139) describes the effect of χ directly. It becomes very clear if one plots the inverse scattering function. Then changes in χ result in parallel shifts of the curves only. Figure 4.32 depicts the results of model calculations for a block copolymer with a volume fraction of polystyrene blocks of $\phi = 0.22$, in correspondence to the sample of Fig. 4.31. The curves were obtained for the indicated values of the product χN_AB.

Obviously the calculations represent the main features correctly: They yield a peak at a certain q_max, which grows in intensity with increasing χ, i.e., with decreasing temperature. The important result comes up for $\chi N_\mathrm{AB} = 21.4$. For this value we find a diverging intensity at the position of the peak, $S(q_\mathrm{max}) \to \infty$. This is exactly the signature of a critical point. We thus realize that the RPA equation formulates a critical transition with a continuous passage from the homogeneous to the ordered phase. When dealing with critical phenomena, it is always important to see the order parameter. Here it is

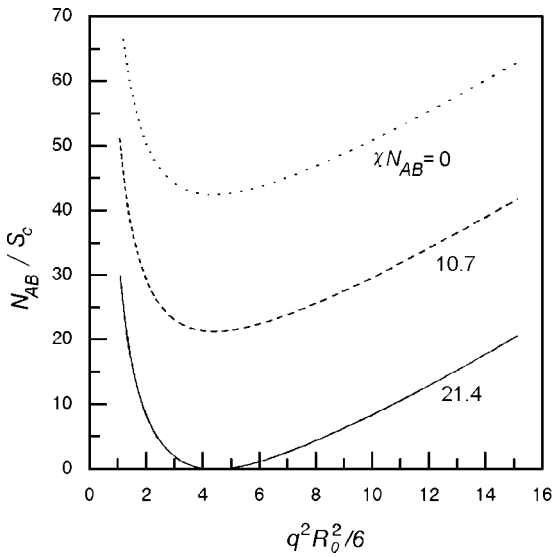

Fig. 4.32. Theoretical scattering functions of a block copolymer with $\phi = 0.22$, calculated for the indicated values of χN_AB

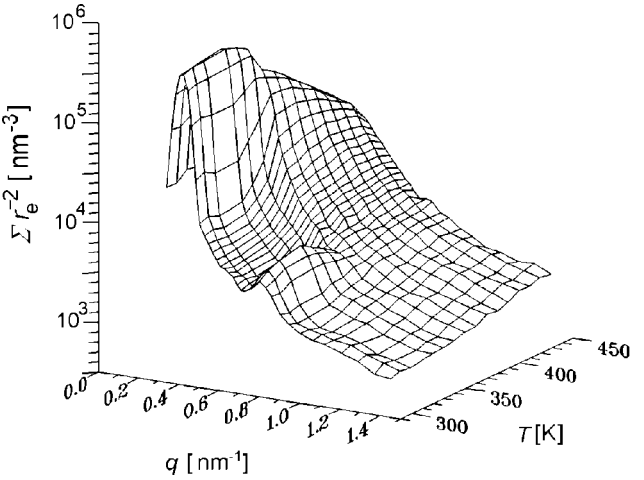

Fig. 4.33. SAXS curves measured for a PS-*block*-PI (ϕ(PS) = 0.44, $M = 1.64 \times 10^4\,\mathrm{g\,mol^{-1}}$) in the temperature range of the microphase separation. The transition occurs at $T_\mathrm{t} = 362\,\mathrm{K}$. Data from Stühn et al. [32]

of a peculiar nature. According to the observations it is associated with the amplitudes of the concentration waves with $|\boldsymbol{k}| = q_\mathrm{max}$.

For $\phi = 0.22$, the critical point is reached for $N_\mathrm{AB}\chi = 21.4$. With the aid of the RPA result, Eq. (4.140), one can calculate the critical values for all ϕ's. In particular, for a symmetric block copolymer one obtains

$$\chi N_\mathrm{AB} = 10.4\,.$$

This is the lowest possible value and the one mentioned in Eq. (4.122).

In polymer mixtures, one calls the curve of points in the phase diagram, where $S(q = 0)$ apparently diverges, the spinodal. One can use the same notion for block copolymers and determine this curve in an equal manner by a linear extrapolation of scattering data measured in the homogeneous phase. We again denote this spinodal by $T_\mathrm{sp}(\phi)$.

Regarding all these findings, one could speculate that the microphase separation might take place as a critical phase transition in the strict sense, at least for block copolymers with the critical composition associated with the lowest transition temperature. In fact, experiments that pass over the phase transition show that this is not true and they also point to other limitations of the RPA treatment. Figure 4.33 presents scattering curves obtained for a polystyrene-*block*-polyisoprene near to the critical composition (ϕ(PS) = 0.44) in a temperature run through the transition point. As we can see, the transition is not continuous up to the end but is associated with the sudden appearance of two Bragg reflections. Hence, although the global behavior is dominated by the steady growth of the concentration fluctuations

typical for a critical behavior, finally there is a discontinuous step, which converts this transition into one of **weakly first order**.

There exists another weak point in the RPA equation. As a basic assumption, it implies that chains in the homogeneous phase maintain Gaussian statistical properties up to the transition point. The reality is different and this is not at all surprising: An increasing tendency for an association of the junction points also necessarily induces a stretching of chains, for the same steric reasons that in the microphase separated state lead to the specific power law Eq. (4.138). This tendency is shown by the data presented in Fig. 4.33 and, even more clearly, by the results depicted in Fig. 4.31. In both cases, $q_{\max}$ shifts to smaller values with decreasing temperature, as is indicative for chain stretching.

The details of the transition are interesting. Figure 4.34 depicts the temperature dependence of the inverse peak intensity $I^{-1}\ (q_{\max})$.

Equation (4.139) predicts a dependence

$$S(q_{\max})^{-1} \propto \chi_{\rm sp} - \chi\ , \tag{4.142}$$

or, assuming a purely enthalpic χ with $\chi \propto 1/T$ (Eq. (4.22)),

$$S(q_{\max})^{-1} \propto T_{\rm sp}^{-1} - T^{-1}\ . \tag{4.143}$$

The findings, however, are different. We can see that the data follow a linear law only for temperatures further away from the transition point and then

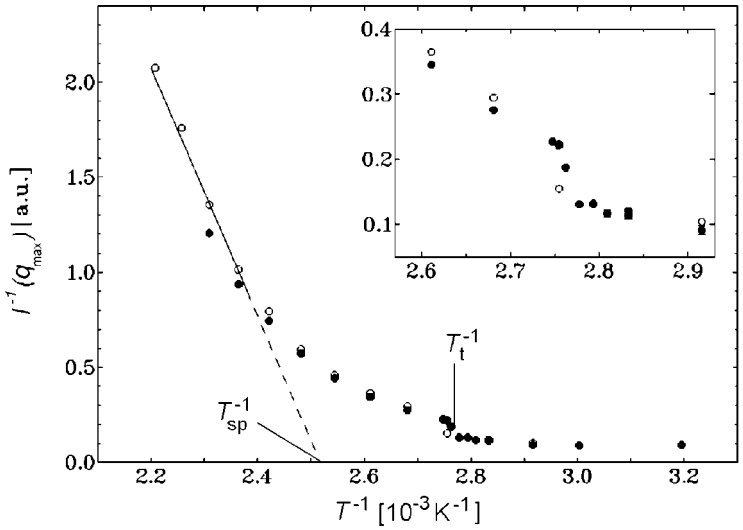

Fig. 4.34. Measurements shown in Fig. 4.33: Temperature dependence of the reciprocal peak intensity, showing deviations from the RPA predictions. The linear extrapolation determines the spinodal temperature

deviate towards higher values. The transition is retarded and does not take place until a temperature 35 K below the spinodal point is reached. According to theoretical explanations, which we cannot further elaborate on here, the phenomenon is due to a lowering of the Gibbs free energy, caused by the temporary short-range order associated with the fluctuations. The short-range order implies local segregations and thus a reduction of the number of AB-contacts, which in turn lowers the Gibbs free energy. We came across this effect earlier in the discussion of the causes of the energy lowering observed in computer simulations of low molar mass mixtures. Remember that there the effect exists only for low enough molar masses, since for high molar masses a short-range ordering becomes impossible. The same prerequisite holds for block copolymers and this is also formulated by the theories.

The short-range ordering is even more pronounced for asymmetric block-copolymers with $\phi_A \ll \phi_B$, which form in the microphase separated state

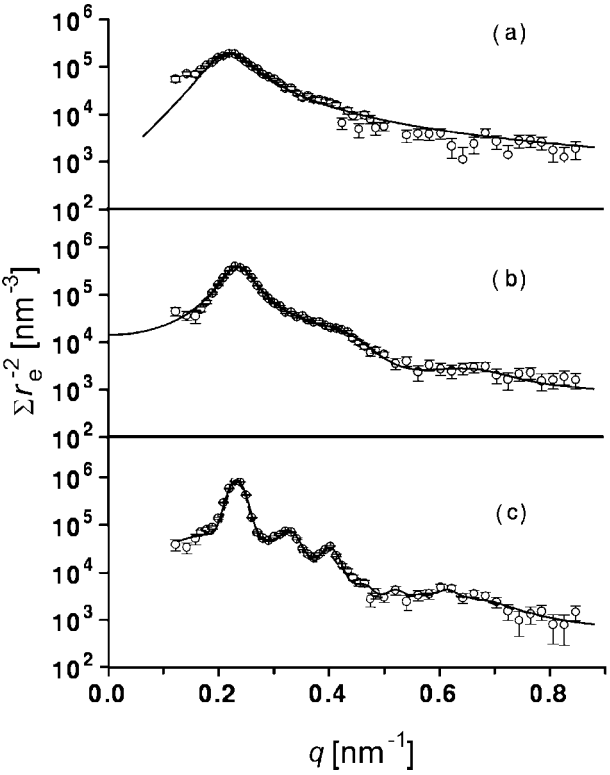

Fig. 4.35. PS-*block*-PI (ϕ(PS) = 0.11): (**a**) Scattering curves referring to the homogeneously disordered state (T = 458 K), (**b**) the state of liquid-like order between spherical domains (T = 413 K), and (**c**) the bcc ordered state (T = 318 K). The *continuous lines* are fits of structural models for the different states of order. From Schwab and Stühn [33]

a bcc-lattice of spheres. The fluctuation-affected temperature range between T_{sp} and T_t is even larger and the short-range ordering here shows up quite clearly in the scattering curves. Figure 4.35(b) presents as an example the scattering curve obtained for polystyrene-*block*-polyisoprene ($\phi(PS) = 0.11$) at $T = 413\,K$ ($T_{sp} = 450\,K$, $T_t = 393\,K$) in a comparison with scattering curves measured above T_{sp} in the homogeneous phase (a) and in the microphase separated state respectively (c). Curve (c) shows the Bragg reflections of a bcc-lattice and the data points in (a) are perfectly reproduced by the RPA equation. Interestingly, the data points in (b) are well-represented by a curve calculated for the scattering of hard spheres with liquid-like ordering; the continuous line drawn through the data points was obtained using the Perkus–Yevick theory, which deals with such liquids. Hence, the ordering during cooling of this block copolymer proceeds in two steps, beginning with the formation of spherical domains that are then placed at the positions of a lattice. The second step takes place when the repulsive interaction reaches a critical value.

Further Reading

K. Binder: *Spinodal Decomposition* in P. Haasen (Ed.): Material Science and Technology, Vol. 5 *Phase Transitions in Materials*, VCH Publishers, 1991

P.J. Flory: *Principles of Polymer Chemistry*, Cornell University Press, 1953

P.-G. de Gennes: *Scaling Concepts in Polymer Physics*, Cornell University Press, 1979

I. Goodman: Developments in Block Copolymers, Vol. 1, Applied Science Publishers, 1982

I. Goodman: Developments in Block Copolymers, Vol. 2, Applied Science Publishers, 1985

I. Hamley: *Block Copolymers*, Oxford University Press, 1999

T. Hashimoto: *Structure Formation in Polymer Systems by Spinodal Decomposition* in R.M. Ottenbrite, L.A. Utracki, S. Inoue (Eds.): Current Topics in Polymer Science, Vol. 2, Hanser, 1987

D.R. Paul, S. Newman (Eds.): *Polymer Blends, Vols. 1 and 2*, Academic Press, 1978